EXHIBIT L – PART 1

U.S. DEPARTMENT OF THE INTERIOR
U.S. GEOLOGICAL SURVEY

Simulation of Ground-Water Flow and Land Subsidence, Antelope Valley Ground-Water Basin, California

Water-Resources Investigations Report 03-4016

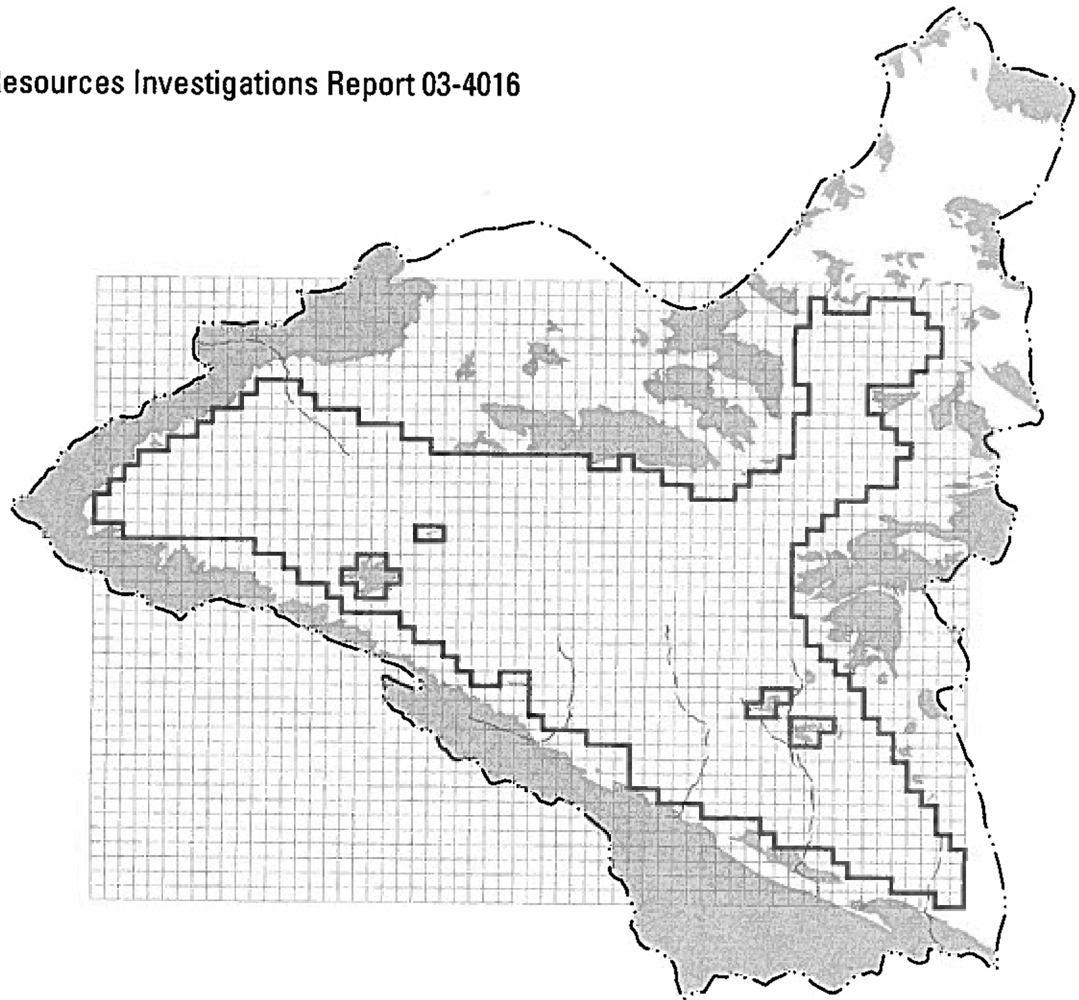

Prepared in cooperation with the **Antelope Valley Water Group**

USGS
science for a changing world

Simulation of Ground-Water Flow and Land Subsidence in the Antelope Valley Ground-Water Basin, California

By David A. Leighton and Steven P. Phillips

U.S. GEOLOGICAL SURVEY

Water-Resources Investigations Report 03-4016

Prepared in cooperation with the

ANTELOPE VALLEY WATER GROUP

Sacramento, California
2003

U.S. DEPARTMENT OF THE INTERIOR

GALE A. NORTON, *Secretary*

U.S. GEOLOGICAL SURVEY

Charles G. Groat, *Director*

For additional information write to:

District Chief
U.S. Geological Survey
Placer Hall—Suite 2012
6000 J Street
Sacramento, California 95819-6129
http://ca.water.usgs.gov

Copies of this report can be purchased from:

U.S. Geological Survey
Information Services
Building 810
Box 25286, Federal Center
Denver, CO 80225-0286

CONTENTS

FIGURES

TABLES

CONVERSION FACTORS, VERTICAL DATUM, AND ABBREVIATIONS

CONVERSION FACTORS

Multiply	By	To obtain
acre	0.4047	hectare
acre-foot (acre-ft)	1,233	cubic meter
acre-foot per year (acre-ft/yr)	1,233	cubic meter per year
foot (ft)	0.3048	meter
foot per day (ft/d)	0.3048	meter per day
foot per year (ft/yr)	0.3048	meter per year
square foot per day (ft^2/d)	0.09290	square meter per day
gallon per minute per foot [(gal/min)/ft)]	0.2070	liter per second per meter
inch (in.)	2.54	centimeter
inch per year (in./yr)	25.4	millimeter per year
mile (mi)	1.609	kilometer
square mile (mi^2)	259.0	hectare

Temperature in degrees Fahrenheit (°F) may be converted to degrees Celsius (°C) as follows:

$$°C = (°F - 32) / 1.8.$$

Vertical Datum

Sea level: In this report, "sea level" refers to the National Geodetic Vertical Datum of 1929 (NGVD of 1929)—a geodetic datum derived from a general adjustment of the first-order level nets of both the United States and Canada, formerly called Sea Level Datum of 1929.

Abbreviations

AVEK	Antelope Valley/East Kern Water Agency
AVWG	Antelope Valley Water Group
BCF	Block-Centered Flow Package
CDPW	California Department of Public Works
CDWR	California Department of Water Resources
CIMIS	California Irrigation Management Information System
HFB	Horizontal Flow Barrier Package
IBS1	Interbed Storage 1 Package
INSAR	interferometric synthetic apecture radar
MODFLOW	modular three-dimensional finite-difference ground-water flow model
SWP	state water project
SWRCB	State Water Resources Control Board (California)

UCCE	University of California Cooperative Extension
USGS	U.S. Geological Survey
d^{-1}	per day
ft^{-1}	per foot

WELL-NUMBERING SYSTEM

Wells are identified and numbered according to their location in the rectangular system for the subdivision of public lands. Identification consists of the township number, north or south; the range number, east or west; and the section number. Each section is divided into sixteen 40-acre tracts lettered consecutively (except I and O), beginning with "A" in the northeast corner of the section and progressing in a sinusoidal manner to "R" in the southeast corner. Within the 40-acre tract, wells are sequentially numbered in the order they are inventoried. The final letter refers to the base line and meridian. In California, there are three base lines and meridians; Humboldt (H), Mount Diablo (M), and San Bernardino (S). All wells in the study area are referenced to the San Bernardino base line and meridian (S). Well numbers consist of 15 characters and follow the format 007N012W27F005S. In this report, well numbers are abbreviated and written 7N/12W-27F5. Wells in the same township and range are referred to only by their section designation, 27F5. The following diagram shows how the number for well 7N/12W-27F5 is derived.

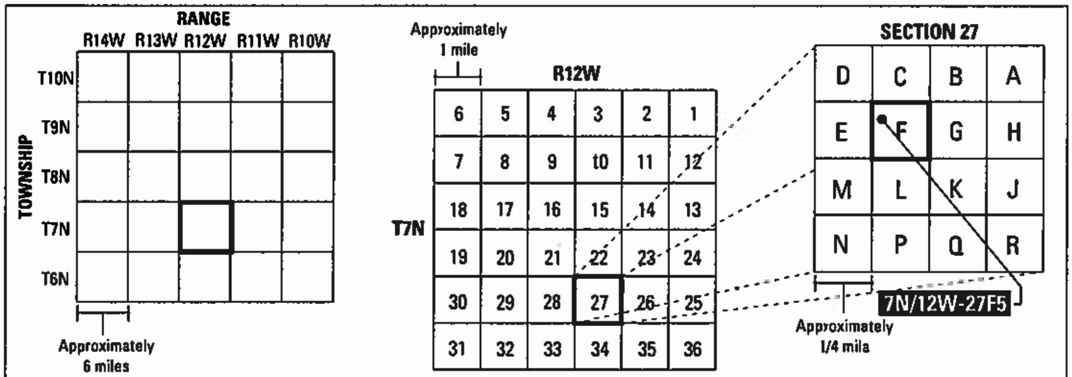

Well-numbering diagram (Note: maps in this report use abbreviated well numbers such as "27F5")

Simulation of Ground-Water Flow and Land Subsidence in the Antelope Valley Ground-Water Basin, California

By David A. Leighton *and* Steven P. Phillips

ABSTRACT

Antelope Valley, California, is a topographically closed basin in the western part of the Mojave Desert, about 50 miles northeast of Los Angeles. The Antelope Valley ground-water basin is about 940 square miles and is separated from the northern part of Antelope Valley by faults and low-lying hills. Prior to 1972, ground water provided more than 90 percent of the total water supply in the valley; since 1972, it has provided between 50 and 90 percent. Most ground-water pumping in the valley occurs in the Antelope Valley ground-water basin, which includes the rapidly growing cities of Lancaster and Palmdale. Ground-water-level declines of more than 200 feet in some parts of the ground-water basin have resulted in an increase in pumping lifts, reduced well efficiency, and land subsidence of more than 6 feet in some areas. Future urban growth and limits on the supply of imported water may continue to increase reliance on ground water. To better understand the ground-water flow system and to develop a tool to aid in effectively managing the water resources, a numerical model of ground-water flow and land subsidence in the Antelope Valley ground-water basin was developed using old and new geohydrologic information.

The ground-water flow system consists of three aquifers: the upper, middle, and lower aquifers. The aquifers, which were identified on the basis of the hydrologic properties, age, and depth of the unconsolidated deposits, consist of gravel, sand, silt, and clay alluvial deposits and clay and silty clay lacustrine deposits. Prior to ground-water development in the valley, recharge was primarily the infiltration of runoff from the surrounding mountains. Ground water flowed from the recharge areas to discharge areas around the playas where it discharged either from the aquifer system as evapotranspiration or from springs. Partial barriers to horizontal ground-water flow, such as faults, have been identified in the ground-water basin. Water-level declines owing to ground-water development have eliminated the natural sources of discharge, and pumping for agricultural and urban uses have become the primary source of discharge from the ground-water system. Infiltration of return flows from agricultural irrigation has become an important source of recharge to the aquifer system.

The ground-water flow model of the basin was discretized horizontally into a grid of 43 rows and 60 columns of square cells 1 mile on a side, and vertically into three layers representing the upper, middle, and lower aquifers. Faults that were thought to act as horizontal-flow barriers were simulated in the model. The model was calibrated to simulate steady-state conditions, represented by 1915 water levels and transient-state conditions during 1915–95 using water-level and subsidence data. Initial estimates of the aquifer-system properties and stresses were obtained from a previously published numerical model of the Antelope Valley ground-water basin; estimates also were obtained from recently collected hydrologic data and from results of simulations of ground-water flow and land subsidence models of the Edwards Air Force Base area. Some of these initial estimates were modified during model calibration. Ground-water pumpage for agriculture

was estimated on the basis of irrigated crop acreage and crop consumptive-use data. Pumpage for public supply, which is metered, was compiled and entered into a database used for this study. Estimated annual pumpage peaked at 395,000 acre-feet (acre-ft) in 1952 and then declined because of declining agricultural production. Recharge from irrigation-return flows was estimated to be 30 percent of agricultural pumpage; the irrigation-return flows were simulated as recharge to the regional water table 10 years following application at land surface. The annual quantity of natural recharge initially was based on estimates from previous studies. During model calibration, natural recharge was reduced from the initial estimate of 40,700 acre-ft per year (acre-ft/yr) to 30,300 acre-ft/yr.

Results of the model simulations indicate that ground-water storage declined more than 8.5 million acre-ft from 1915 to 1995. During the period of peak pumping (1949–53), pumpage averaged 363,000 acre-ft/yr, and 79 percent of the ground water withdrawn came from storage primarily from layer 1 (the upper aquifer). Water released from compaction of the aquitards accounted for about 21,600 acre-ft/yr of the ground water removed from storage. Downward leakage from layer 1 into layer 2 (the middle aquifer) accounted for most (86 percent) of the pumpage from layer 2. For the simulation period 1991–95 (a period representing current conditions when pumpage for public supply exceeded agricultural pumpage), pumpage averaged 81,700 acre-ft/yr, and most of the ground water withdrawn from layer 2 came from downward leakage from layer 1. During this period, ground water removed from storage accounted for 17 percent of the total pumpage and recharge from irrigation return accounted for about 39 percent of the total pumpage. Ground water removed from storage as a result of compaction of aquitards was reduced to about 3,800 acre-ft/yr.

The calibrated model was used to simulate the response of the aquifer to future pumping scenarios. Results of the simulation of scenario 1, for which total annual pumpage for 1996–2025 remained at the level specified for 1995, showed that water levels continued to rise (as much as 36 feet) in agricultural areas, continuing the long-term recovery from drawdown caused by historical agricultural pumpage. In the areas where pumping for public supply is concentrated, water levels continued to decline and subsidence continued in the central part of the ground-water basin. Water-level declines were largest (more than 100 feet) in the south-central part of the ground-water basin; most of the public-supply pumpage occurs in this area. As much as 1.9 feet of additional subsidence was simulated in the central part of the ground-water basin from 1996 to 2025. For scenario 2, public-supply pumpage was increased by 3.3 percent annually, and annual agricultural pumpage was increased by 75 percent more than that specified for 1995. Pumpage increases for scenario 2 resulted in significant water-level declines in the southern and northeastern part of the Lancaster subbasin; most pumping for public supply occurs in these areas. Results of this simulation showed that water levels declined more than 150 feet in the south-central part of the ground-water basin and that an additional 5 feet of subsidence was simulated in the central part of the basin.

INTRODUCTION

Ground water is an important component of the water supply in Antelope Valley. Prior to 1972, ground water provided more than 90 percent of the total water supply in the valley. From the mid 1960s through the mid 1980s, ground-water pumpage declined owing to declines in agricultural production and, beginning in 1972, availability of imported water from the State Water Project (SWP). This steady decline in ground-water pumpage ceased in the mid 1980s due to increased urban growth and the associated demand for ground water. Since 1972, between 50 and 90 percent of the total water demand in the valley has been met using ground water (Templin and others, 1995). Ground-water-level declines have increased pumping lifts, reduced well efficiency, and caused aquifer-system compaction and more than 6 ft of land subsidence in some areas (Ikehara and Phillips, 1994). Projected urban growth and limits on the available imported water may continue to increase the reliance on ground water and exacerbate aquifer-system compaction and land subsidence (Galloway and others, 1998).

Projections of water supply and demand indicate that the current supply may fall short of demand early in the 21st century (Kennedy/Jenks, 1995). Conjunctive use of surface and ground water, along with methods that can enhance or better use the ground-water resource, will likely become an important part of water-resource management in Antelope Valley. A thorough understanding of the ground-water system is needed to effectively manage the ground-water resource.

In the 1970s, the U.S. Geological Survey (USGS) developed a numerical ground-water flow model that was used by water managers to help make decisions regarding imported water from the SWP, reclaimed wastewater, and captured floodwater (Durbin, 1978). Since the development of this model, ground-water use in the valley has decreased substantially, and areas of ground-water withdrawals have changed from primarily agricultural areas to primarily urban areas. These changes in the state of the ground-water system emphasize the need for a better understanding of the system and the effects of water-management practices.

Purpose and Scope

In 1992, the USGS began working with the Antelope Valley Water Group (AVWG) to provide information needed to manage the water resources in Antelope Valley. Results from two studies completed as part of that work are presented in reports by Templin and others (1995) and Ikehara and Phillips (1994). Templin and others (1995) describes land use, water supply and demand (1919–91), and water demand forecasts in the Antelope Valley. Ikehara and Phillips (1994) describes land subsidence and its relation to ground-water withdrawals. The results of these studies and improvements in modeling capabilities, combined with data collected since the development of the ground-water flow model of Antelope Valley in the 1970's (Durbin, 1978), have made it possible to develop an updated numerical model of ground-water flow in Antelope Valley that includes the simulation of aquifer-system compaction and land subsidence. The model was developed to assist Antelope Valley water managers and planners.

The purpose of this report is to describe a conceptual model of the Antelope Valley ground-water basin, to describe the development and calibration of a numerical model of ground-water flow, aquifer-system compaction, and land subsidence, and to present results of simulated future pumping scenarios being considered by water managers. Available geohydrologic data and data collected during this study were used to develop the revised conceptual model of the flow system that forms the basis of the revised, updated numerical model of the Antelope Valley ground-water basin. The numerical model was calibrated and simulates ground-water flow, aquifer-system compaction, and land subsidence using water-level data for 1915–95 and land subsidence data for 1926–92. The model was used to provide insight into the geohydrology of the Antelope Valley ground-water basin, to test the sensitivity of the new model to aquifer-system parameters and hydrologic stresses, and to compare the potential effects of future pumping scenarios. Further, the results of this study can be used to guide future data-collection and aid in making informed water-management decisions.

Description of Study Area

Antelope Valley, which is located in parts of Kern, Los Angeles, and San Bernardino Counties in the western part of the Mojave Desert, is about 50 mi northeast of Los Angeles (fig. 1). The valley is bounded on the south by the southeast-trending San Gabriel Mountains and on the northwest by the northeast-trending Tehachapi Mountains. The northern and eastern boundaries of the valley are formed by lower hills, ridges, and buttes. The valley is a topographically closed basin and the valley floor slopes gently toward several playas; surface-water runoff terminates in these playas. The altitudes of the valley floor, the interior hills, and the foothills range from 2,270 to 3,500 ft above sea level, and the surrounding mountains rise as high as 10,064 ft above sea level.

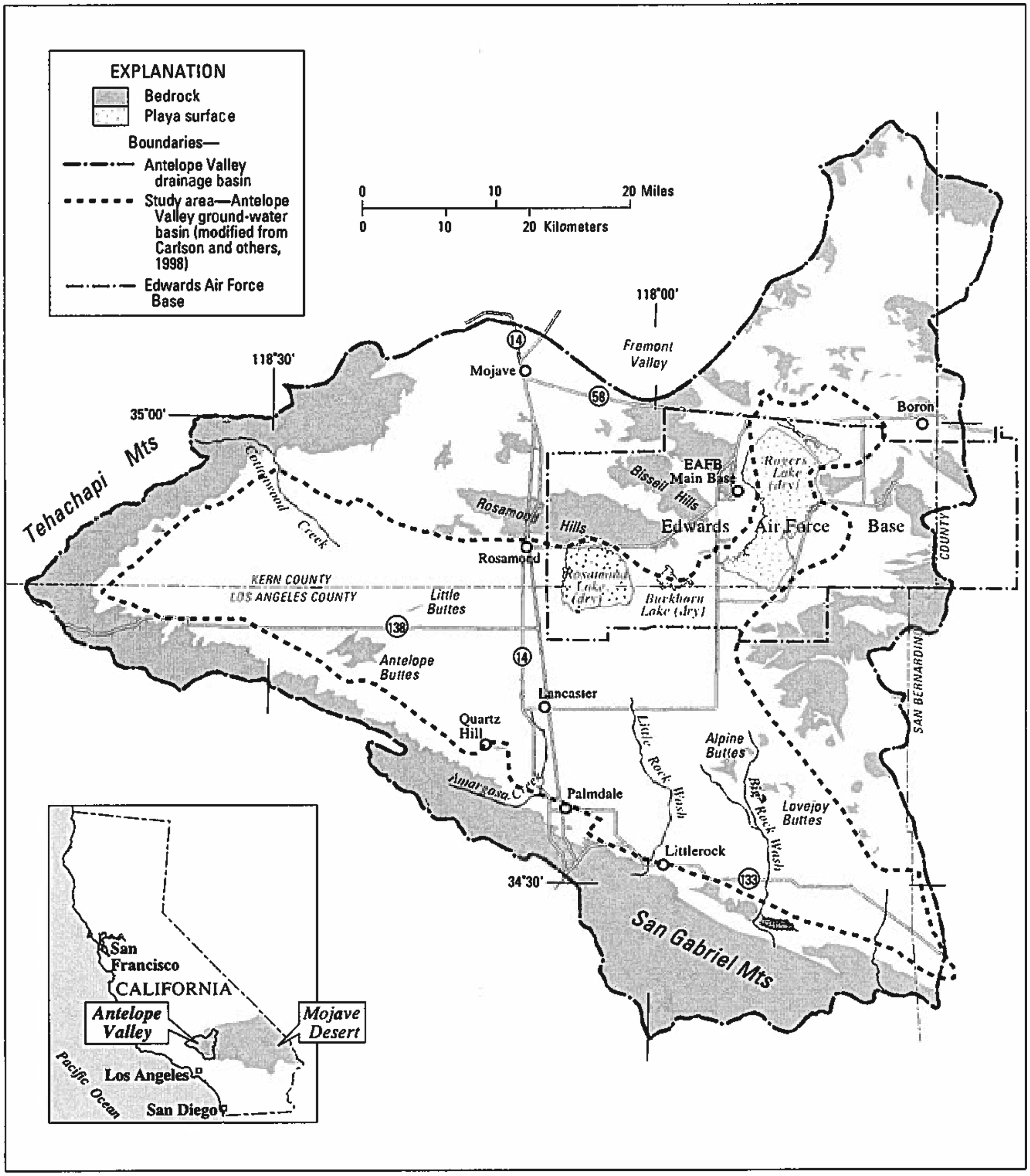

Figure 1. Location of study area, Antelope Valley, California.

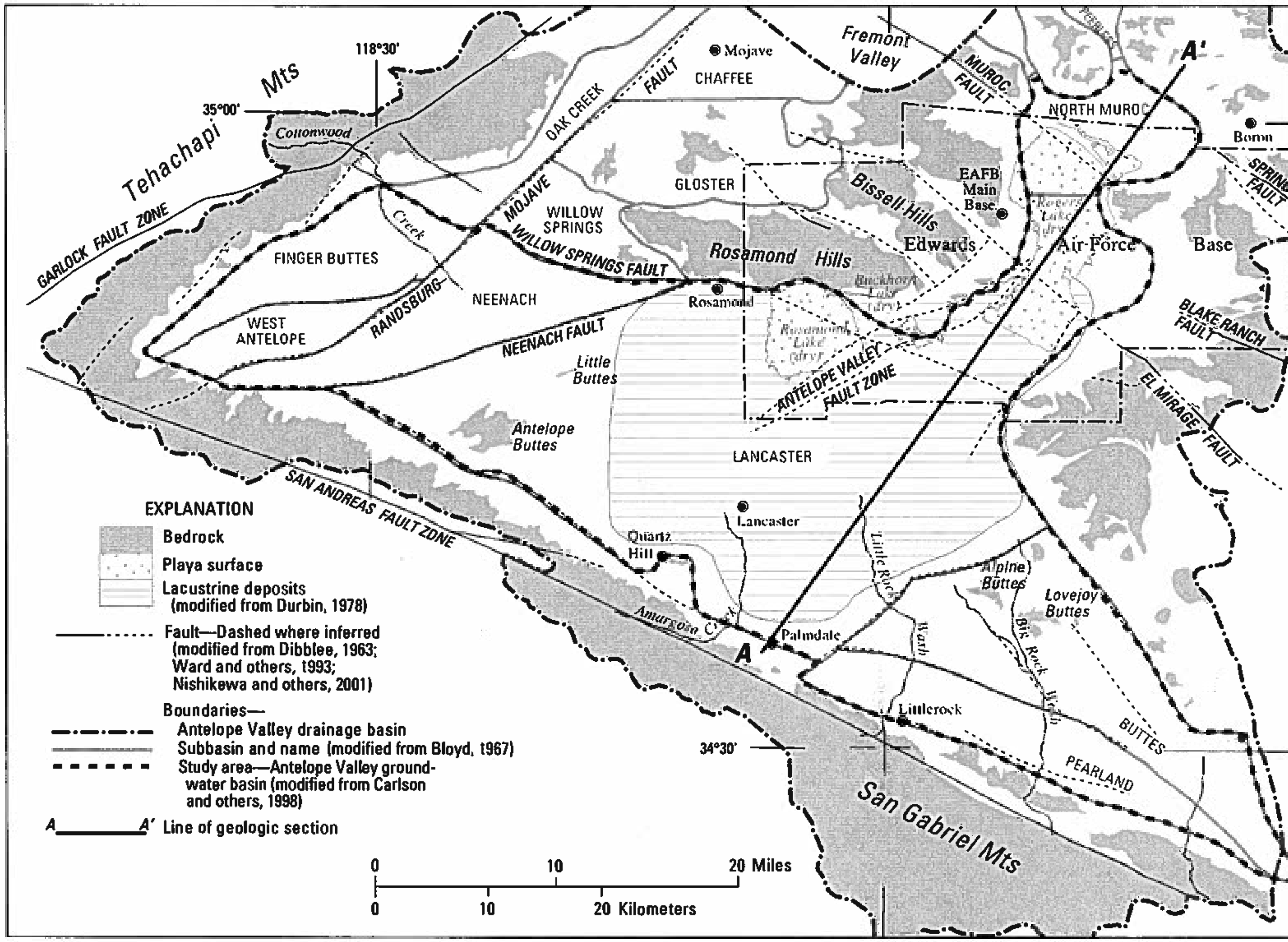

Figure 2. Location of faults, ground-water subbasins, line of geologic section, and approximate areal extent of lacustrine deposits in the Antelope Valley ground-water subbasin, California.

The climate in the study area is semiarid to arid. Average annual precipitation in the interior of the valley is less than 10 in. (Rantz, 1969), humidity is low, and temperatures range from below 32°F in the winter to more than 100°F in the summer. Most precipitation occurs between October and March. Land use in the valley is primarily urban, agricultural, industrial, and military. Lancaster and Palmdale are the largest cities in the valley; in 1988, they had a combined population of about 244,000 (California Department of Finance, 1998).

The Antelope Valley ground-water basin, which is the focus of this report, was defined by Carlson and others (1998) and is part of the Antelope Valley drainage basin (fig. 2). The Antelope Valley drainage basin has been divided into 12 ground-water subbasins (fig. 2) on the basis of faults, consolidated rocks, ground-water divides, and, in some cases, arbitrary boundaries (Thayer, 1946; Bloyd, 1967). The Antelope Valley ground-water basin covers about 920 mi^2, and consists of seven of these subbasins; the Buttes, Finger Buttes, Lancaster, Neenach, North Muroc, Pearland, and West Antelope (fig. 2). The Lancaster subbasin is the largest and most developed of the subbasins.The Antelope Valley ground-water basin is separated from the northern part of Antelope Valley by faults and low-lying hills. Most of the urban and agricultural development and associated ground-water pumping in Antelope Valley occurs within the study area.

Acknowledgments

The authors gratefully acknowledge the members of the Antelope Valley Water Group for their assistance during this study. They provided data, local knowledge, and advice that were important to the successful completion of the study. We also thank Loren Metzger of the USGS for his invaluable assistance in compiling the water-use data.

GEOHYDROLOGY

The geohydrology of Antelope Valley is described in detail by previous investigators. The general geologic structure of Antelope Valley was inferred on the basis of a gravity survey by Mabey (1960). The surficial geology of the valley was mapped and described by Dibblee (1952, 1957, 1958a, 1958b, 1959a, 1959b, 1959c, 1959d, 1960a, 1960b, 1963, 1967, 1981) and Noble (1953). Surveys by Johnson (1911) and Thompson (1929) provide information on ground-water conditions during the early ground-water development. Additional studies on the ground-water resources in Antelope Valley are documented in reports by Thayer (1946), the California Department of Water Resources (1947), the California Department of Public Works (1955), Snyder (1955), Dutcher and Worts (1963), Weir and others (1965), Bloyd (1967), Duell (1987), Londquist and others (1993), Rewis (1995), Carlson and others (1998), Carlson and Phillips (1998), and Nishikawa and others (2001). The geohydrology of Antelope Valley is summarized in the following sections, but the reader is referred to the aforementioned reports for a more detailed description.

Geologic Setting

Underlying Antelope Valley are large sediment-filled structural depressions that are downfaulted between the Garlock and the San Andreas Fault zones. The bedrock complex in the valley forms the margins and the base of the ground-water basin and crops out in the highlands that surround the valley. This bedrock complex consists of pre-Cenozoic igneous rocks and consolidated Tertiary sedimentary rocks (Hewett, 1954; Dibblee, 1963).

In the Antelope Valley ground-water basin, a series of unconsolidated deposits of Quaternary age, some more than 5,000 ft thick (Benda and others, 1960; Mabey, 1960; R.C. Jachens, U.S. Geological Survey, written commun., 1991), overlies consolidated rocks and forms the basin fill. On the basis of the mode of deposition, Dutcher and Worts (1963) mapped these deposits as either alluvial or lacustrine. The alluvium consists of unconsolidated to moderately indurated, poorly sorted gravels, sands, silts, and clays. The older deep units within the alluvium typically are more compacted and indurated than the younger shallow units (Dutcher and Worts, 1963; Durbin, 1978). The fine-grained lacustrine deposits consist of sands, silts, and clays that accumulated in a large lake or marsh that at times covered large parts of the study area (Dibblee, 1967). These lacustrine deposits consist primarily of thick layers of blue-green silty clay, known locally as the blue clay member of the lacustrine deposits

(Dutcher and Worts, 1963), and a brown clay containing thin interbedded layers of sand and silt. Individual clay beds are as much as 100 ft thick and are interbedded with lenses of coarser material as much as 20 ft thick. The entire sequence of lacustrine deposits is as much as 300 ft thick in some areas (Dutcher and Worts, 1963). These deposits are overlain by as much as 800 ft of alluvium in the southern part of the Lancaster subbasin near Palmdale, become progressively shallower northward, and are exposed at the surface near the southern edge of Rogers Lake. Alluvial fans that were formed by the erosion of materials from the San Gabriel Mountains encroached upon an ancient lake where the lacustrine deposits were accumulating, forcing the the ancient lake, and associated lacustrine deposits, northward with time (Durbin, 1978). The areal extent of the lacustrine deposits is not well defined, but its approximate extent is shown in figure 2.

Antelope Valley contains numerous faults (fig. 2), some of which act as partial barriers to ground-water flow. Most of these faults are described in reports by Mabey (1960), Dibblee (1960b, 1963), Dutcher and Worts (1963), and Ward and others (1993). More recent data and analysis have extended previously described faults and identified a previously unknown fault. Nishikawa and others (2001) suggest that the Muroc and the El Mirage Faults extend across Rogers Lake (fig. 2); the extensions of these faults were based on water-level data and results from sub-regional ground-water flow simulations. Nishikawa and others (2001) also identified a fault that trends from the northwest corner of Rosamond Lake southeast along the southern edge of Buckhorn Lake to the eastern edge of the study area (fig. 2). This fault, which may be an extension of the Willow Springs Fault, was inferred on the basis of water-level data; water levels are as much as 65 ft lower on the northeast side of the fault than on the southwest side. Large water-level differences between nearby wells in the Buttes subbasin suggest the existence of a previously unknown fault; this fault is thought to trend southeast of Lovejoy Buttes, parallel to the northeastern boundary of the Buttes subbasin (fig. 2).

Aquifer System and Boundaries

The lateral boundaries of the Antelope Valley ground-water basin are formed, in most cases, by shallow or exposed bedrock. North of the Finger Buttes and the Neenach subbasins, the boundary of the ground-water basin is formed by the Willow Springs Fault (fig. 2). This fault is assumed to be an effective barrier to ground-water flow to and from subbasins to the north (Durbin, 1978). This assumption is supported by evidence that springs existed along the fault prior to ground-water development and, more recently, by large water-level differences over short distances across the fault (Carlson and others, 1998).

The historical conceptual model of the aquifer system in the Antelope Valley ground-water basin utilized a lithostratigraphic approach to divide the basin sediments into two major aquifers; an upper unconfined aquifer known locally as the "principal" aquifer and a "deep" aquifer overlain and confined by lacustrine deposits (Dutcher and Worts, 1963; Bloyd, 1967; Durbin, 1978). The principal aquifer was defined as the aluvial deposits that overlie the lacustrine deposits in the Antelope Valley ground-water basin south and west of Rogers Lake. The principal aquifer was assumed to be unconfined throughout its entire extent. The deep aquifer was defined as the alluvial deposits that underlie the lacustrine deposits throughout the Antelope Valley ground-water basin and the lacustrine and alluvial deposits in the Antelope Valley ground-water basin east and north of Rogers Lake. The deep aquifer was assumed confined in areas where it is overlain by the lacustrine deposits and unconfined to semiconfined in the Rogers Lake area where the principal aquifer and lacustrine deposits were assumed not to exist.

Paleomagnetic analyses of core samples collected during the drilling of monitoring site 7N/12W-27P5–8, south of Lancaster, indicate a change from normal polarity at 344 ft below land surface to reversed polarity at 450 ft below land surface (Fram and others, 2002). This reversal in polarity is interpreted as the transition from the Brunhes to the Matuyama polarity-chronostratigraphic units (John Hillhouse, U.S. Geological Survey, written commun., 1998), which occurred about 780,000 years ago (Cande and Kent, 1995). The lacustrine deposits were encountered at a depth of about 740 ft below land surface at the monitoring site, indicating that these deposits are significantly older than 780,000 years. In contrast, the lacustrine deposits collected from less than 100 ft below land surface at Edwards Air Force Base interfinger with alluvial deposits less than 14,000 years old (Ponti, 1985).Therefore, the historical conceptual model groups alluvial deposits that are younger than 14,000 years with deposits that are older than 780,000 years in the same aquifer. In general, the alluvial deposits become more consolidated and indurated (hardened) with age, which decreases the ability of the aquifer material to transmit and store water. Because the hydraulic properties of the alluvial deposits change with time, the grouping of deposits of significantly different ages into the same aquifer is probably not reasonable.

Stratigraphic, hydrologic, and water-quality data collected since the early 1990s (Londquist and others, 1993; Rewis, 1993; Metzger and others, 2002) were used in this study to redefine the conceptual mode of the Antelope Valley ground-water basin. The new conceptual model utilizes a chronostratigraphic approach instead of a lithostratigraphic approach to divide the ground-water basin into an upper, middle, and lower aquifer. Lithologic and geophysical logs of wells drilled in Lancaster (Metzger and others, 2002) and at Edwards Air Force Base south of Rogers Lake (Londquist and others, 1993; Rewis, 1993) indicate that the alluvial deposits become less permeable and more indurated at approximately 1,950 and 1,550 ft above sea level. These changes in properties were assumed to represent chronostratigraphic boundaries and were used to divide the ground-water basin into the three aquifers. The upper aquifer extends from the water table to an altitude of about 1,950 ft above sea level, the middle aquifer extends from 1,950 to 1,550 ft above sea level, and the lower aquifer extends from 1,550 ft above sea level to the altitude at which bedrock is encountered (fig. 3). Geophysical data are limited or nonexistent elsewhere in the basin and thus it was assumed that these changes in properties of the alluvium with depth were laterally extensive throughout the basin. The lacustrine deposits were assumed to be included in these aquifers.

The upper aquifer varies from unconfined to confined depending on the presence and vertical position of the thick lacustrine deposits within the aquifer. In the south part of the Lancaster subbasin, from Palmdale to where Little Rock Wash crosses section A-A′, the lacustrine deposits are below the upper aquifer, and the upper aquifer generally is unconfined. The upper aquifer may be locally confined in this area and in areas outside the extent of the lacustrine deposits owing to the presence of discontinuous interbedded aquitards. North of Little Rock Wash, the lacustrine deposits are present at shallower depths and are considered a part of the upper aquifer. In the northern part of the study area around Rogers Lake, the lacustrine deposits are exposed at land surface and form the upper part of the upper aquifer. In these areas where the lacustrine deposits are a part of the upper aquifer, the upper aquifer is confined below the lacustrine deposits.

In the southern part of the Lancaster subbasin, where the lacustrine deposits are deepest, the lacustrine deposits are part of the middle aquifer; but in the northern part of the subbasin, these deposits overlie the middle aquifer. Owing to the overlying lacustrine deposits and the discontinuous interbedded aquitards, the middle aquifer is assumed confined. If water levels were to decline below the confining aquitards, the middle aquifer could become unconfined in places.

The alluvium in the lower aquifer becomes increasingly consolidated and indurated with depth and, in the deepest parts of the basin, probably is able to transmit and store only small quantities of water. The lacustrine deposits overlie this aquifer except possibly in areas around Palmdale and Lancaster where the lacustrine may be partly contained within the lower aquifer. The lower aquifer is confined by the overlying lacustrine deposits and the discontinuous interbedded aquitards in the middle aquifer.

Pre-Development Conditions

Prior to ground-water development in Antelope Valley, long-term ground-water conditions in the study area were in a state of dynamic equilibrium. That is, on a time scale of several years or decades, average annual natural recharge to the basin was balanced by average annual natural discharge, and ground-water levels generally fluctuated about long-term mean water levels that remained constant over time. Although the equilibrium of recharge and discharge was affected by dry and wet climatic cycles, the equilibrium was maintained over the long term.

Recharge

The primary source of natural recharge to the basin is infiltration of precipitation runoff from the surrounding mountains (primarily from the San Gabriel Mountains south of the valley) in ephemeral stream channels. This recharge, defined as mountain-front recharge, generally occurs at the heads of the alluvial fans and along the stream channels near where the streams enter the valley (fig. 4). During periods of high runoff, these streams can flow onto the valley floor, which may result in some recharge along stream channels and washes. Other sources of natural recharge include direct infiltration of precipitation and lateral ground-water underflow from adjacent bedrock areas and basins, both of which probably are small compared with mountain-front recharge. Precipitation over the valley floor generally is less than 10 in./yr (Rantz, 1969) and evapotranspiration rates [pan evaporation rate is about 114 in./yr (Bloyd, 1967)] and soil moisture requirements are high; therefore, recharge from direct infiltration of precipitation is negligible (Snyder, 1955; Durbin, 1978). Lateral ground-water flow from fractures in adjacent bedrock, from the Willow Springs subbasin south across the Willow Springs Fault, and from other areas adjacent to the study area also may recharge the basin, but the quantity of recharge from these sources is unknown and probably is negligible (Bloyd, 1967).

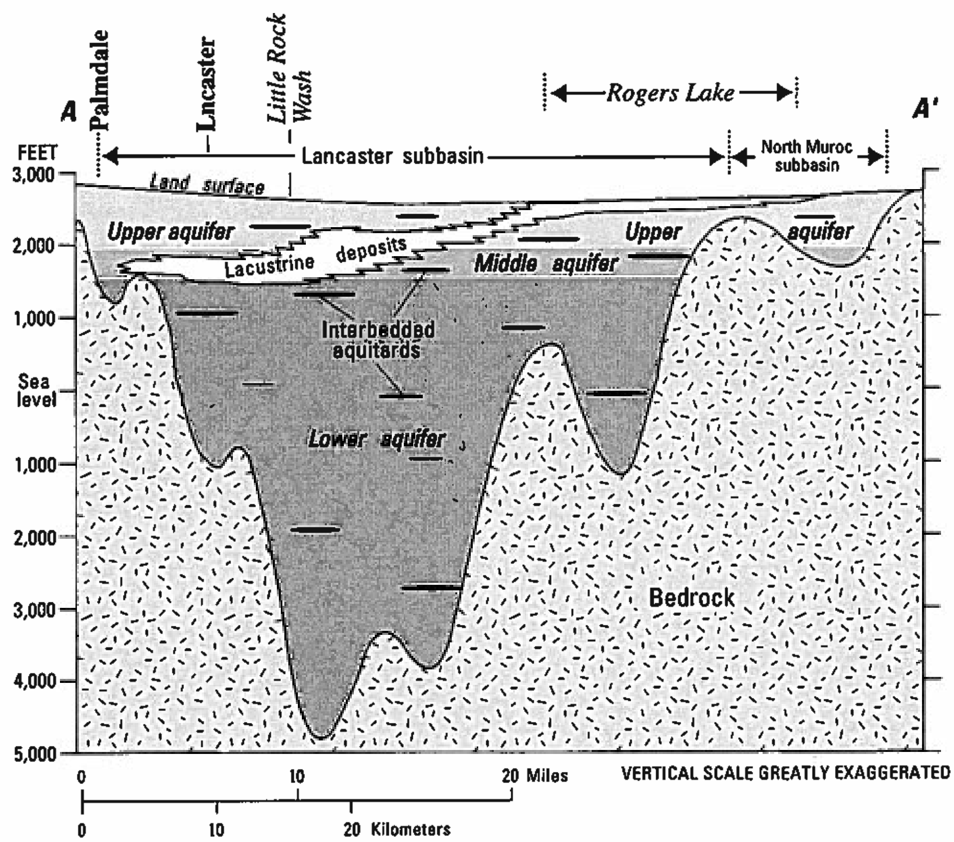

Figure 3. Generalized geologic section showing relation of lacustrine deposits to aquifers in the Lancaster and the North Muroc subbasins in the Antelope Valley ground-water basin, California (modified from Londquist and others, 1993). Line of section is shown on figure 2.

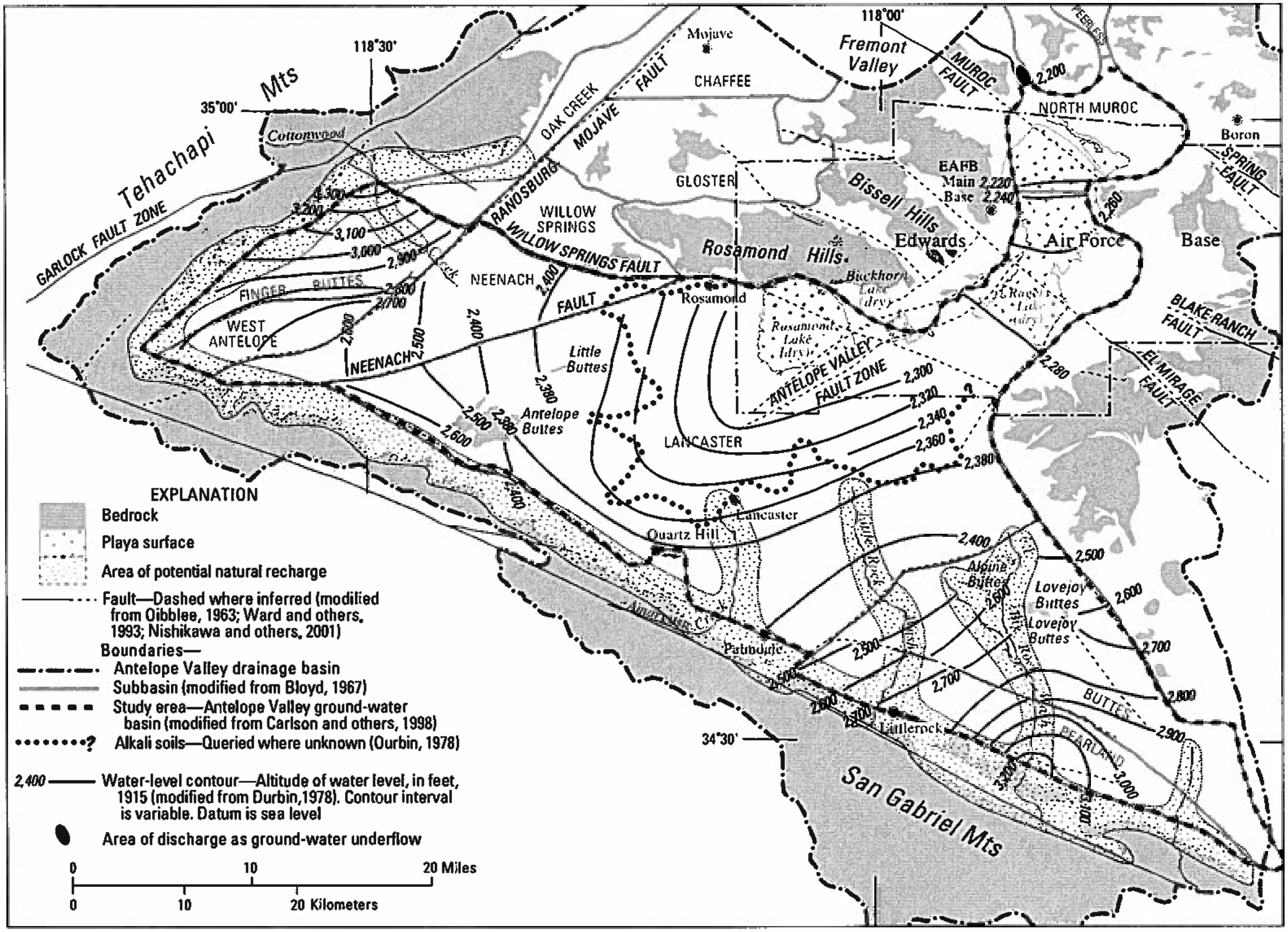

Figure 4. Ground-water levels in 1915 and location of areas of potential natural recharge, natural discharge as ground-water underflow, and alkali soils in the Antelope Valley ground-water basin, California.

The quantity of mountain-front recharge in Antelope Valley was estimated during previous investigations: all estimates were based on rainfall, runoff, and channel-geometry data. Londquist and others (1993) summarized these estimates and concluded that those by Bloyd (1967) and Durbin (1978) probably are the most representative of actual recharge in the valley because their estimates were based on long-term discharge and climatological data. Bloyd (1967) estimated that annual mountain-front recharge was about 58,000 acre-ft using a surface-water drainage area of the entire Antelope Valley (558 mi^2). Durbin (1978) estimated that the annual mountain-front recharge was about 40,700 acre-ft, which is based on the surface-water drainage area of the Antelope Valley ground-water basin (385 mi^2). Bloyd's (1967) and Durbin's (1978) estimates resulted in similar values for mountain-front recharge—104 and 106 acre-ft/mi^2 of surface-water drainage area, respectively. Applying Bloyd's (1967) estimate of recharge per square mile to the surface-water drainage area used by Durbin (1978) resulted in an estimated annual mountain-front recharge of about 40,040 acre-ft for the Antelope Valley ground-water basin, which is similar to Durbin's (1978) estimate of annual mountain-front recharge (40,700 acre-ft). Results from a study of the infiltration of surface runoff in the Mojave River Basin (Izbicki and others, 1995), which is immediately east of Antelope Valley, indicate that recharge from surface runoff in ephemeral streams is limited in this arid environment. Izbicki and others (1995) used water-quality analyses, ground-water age-dating techniques, and ground-water flow modeling to estimate recharge. The results from Izbicki and others (1995) suggest that natural recharge in the Antelope Valley ground-water basin may be less than that estimated by Bloyd (1967) and Durbin (1978).

Discharge

The primary source of discharge of water from the basin prior to ground-water development was from evapotranspiration in the lower parts of the valley where the water table was within 10 ft of land surface (Lee, 1912). The pan evaporation rate in Antelope Valley is about 114 in./yr (Bloyd, 1967) and represents the upper limit of bare-soil evaporation. A large area of alkali soils (fig. 4) (Durbin, 1978) and the existence of phreatophytes in the north central part of the ground-water basin, which require saturated soil within the root zone, indicate that the water table was near land surface at one time and that evapotranspiration was significant (Thompson, 1929). Evapotranspiration by mesquite, a common phreatophyte in the study area, ranges between 0.1 and 1.4 ft/yr, depending on areal density (Lines and Bilhorn, 1996). Durbin (1978) estimated that prior to ground-water development, discharge from the basin owing to evapotranspiration was about 39,400 acre-ft/yr; he based this estimate on a mass balance. Other types of discharge from the basin included lateral ground-water underflow and springs. Bloyd (1967) and Durbin (1978) stated that ground-water underflow occurred through a gap in the bedrock in the northwest corner of the North Muroc subbasin into the Fremont Valley Basin. Bloyd (1967) estimated that 100 to 500 acre-ft/yr and Durbin (1978) estimated that about 1,000 acre-ft/yr flowed through this gap. Discharge by springs was thought to be less than 300 acre-ft/yr (Johnson, 1911; Thompson, 1929).

Post-Development Conditions

Development of the ground-water resource in Antelope Valley has caused significant changes in the amount, distribution, and type of recharge and discharge. New sources of recharge include irrigation return flow and infiltration of treated wastewater, and the primary source of discharge, evapotranspiration, has been replaced by ground-water pumping.

Recharge

Since the development of irrigated agriculture in the Antelope Valley ground-water basin, large amounts of irrigation water have been applied to crops; much of this water may have percolated below the root zone and contributed recharge to the ground-water basin. Snyder (1955) reported that agricultural recharge probably reached the water table by the early 1950s. Durbin (1978), however, assumed that this water had not reached the water table in 1961 based on water-quality data, which indicated that the dissolved-solids concentration in ground water had not changed. He reported that the existence of layers of fine-grained material above the water table may have prevented or delayed the downward migration of this water. Durbin (1978) also reported that the concentration of dissolved solids started to increase in the 1960s, which indicated that irrigation water may have begun to reach the water table. Rising water levels and high nitrate concentrations in areas that historically have been used for agricultural production since the mid 1970s support the assumption that infiltration of irrigation water has contributed recharge to the ground-water basin.

Infiltration of treated wastewater may also contribute recharge to the ground-water basin. The largest producers of treated wastewater in the study area are the Palmdale Water Reclamation Plant and the Lancaster Water Reclamation Plant (Templin and others, 1995). Beginning in 1975, treated wastewater has been disposed of in ponds or on spreading grounds (areas where water is spread over the land surface to evaporate or infiltrate below land surface). A small amount of the treated wastewater is reclaimed and used primarily for agriculture (Templin and others, 1995). The quantity of disposed wastewater available for infiltration and potential recharge was estimated by subtracting estimated evaporation from the quantity of treated wastewater that is disposed of in ponds or on spreading grounds (David Lambert, County Sanitation District of Los Angeles County, written commun., 1996). Treated wastewater from the Palmdale Water Reclamation Plant is spread on approximately 60 acres of land. At the Lancaster Water Reclamation Plant, treated wastewater is disposed of in ponds that encompass about 430 acres. On the basis of a pan evaporation rate of 114 in./yr (9.5 ft/yr) for Antelope Valley (Bloyd, 1967), about 570 acre-ft/yr of the treated wastewater from the Palmdale Water Reclamation Plant and about 4,085 acre-ft/yr of the treated wastewater from the Lancaster Reclamation Plant is lost to evaporation. The annual quantity of treated wastewater discharged to spreading ponds and the estimated potential annual infiltration of wastewater in the ponds are shown in table 1. Results of studies at the Lancaster Water Reclamation Plant indicate that infiltration of the ponded water probably does not reach the regional water table owing to the high clay content of the sediments (David Lambert, County Sanitation District of Los Angeles County, written commun., 1996).

Table 1. Annual treated wastewater discharged to ponds and spreading grounds, and potential annual infiltration of the treated wastewater in the Antelope Valley ground-water basin, 1975–95

[Discharge data from David Lambert (County Sanitation Districts of Los Angeles County, written commun., 1996). acre-ft, acre-feet. —, no data]

Year	Lancaster Water Reclamation Plant		Palmdale Water Reclamation Plant	
	Wastewater discharge (acre-ft)	Potential infiltration of wastewater (acre-ft)	Wastewater discharge (acre-ft)	Potential infiltration of wastewater (acre-ft)
1975	840	0	—	—
1976	1,280	0	—	—
1977	1,700	0	—	—
1978	2,160	0	—	—
1979	1,980	0	—	—
1980	2,170	0	—	—
1981	2,320	0	—	—
1982	2,120	0	—	—
1983	2,770	0	—	—
1984	2,590	0	1,100	530
1985	3,090	0	2,000	1,430
1986	4,210	125	2,580	2,010
1987	5,140	1,055	3,510	2,940
1988	3,660	0	3,730	3,160
1989	2,100	0	3,960	3,390
1990	2,270	0	5,440	4,870
1991	2,410	0	5,110	4,540
1992	3,400	0	6,150	5,580
1993	5,150	1,065	7,080	6,510
1994	4,980	895	7,480	6,910
1995	7,000	2,915	8,070	7,500

Mountain-front recharge is affected by climatic conditions, which have not changed significantly during the years represented by this study. On the basis of the limited data available on mountain-front recharge, we assumed that the quantity of mountain-front recharge probably has remained fairly constant over time. However, the encroachment of land development into areas where mountain-front recharge occurs may affect this source of recharge. Lateral ground-water flow from adjacent areas is being affected by changes in the water-level gradient, but the quantity of lateral flow is small and the changes in this component of natural recharge have little effect on total natural recharge in the basin.

Discharge

The primary form of discharge from the ground-water basin is ground-water pumpage. The use of ground water for irrigation in the Antelope Valley began in the 1800s; but, until about 1915, the quantity of ground-water pumpage was small. Beginning in 1915, the number of wells drilled in Antelope Valley increased significantly resulting in increases in annual pumpage. Historical pumpage was estimated by Snyder (1955), Durbin (1978), California Department of Water Resources (1980, 1990, and 1991), and Templin and others (1995); their estimates are presented in figure 5 along with estimates calculated for this current study. The large differences in the estimates of pumpage may be due to differences in the methods used to estimate pumpage and in the area represented by the estimate. In 1919, pumpage was estimated to be about 31,000 acre-ft (California Department of Water Resources, 1980). By the early to mid 1950s, pumpage had increased to its highest levels; estimates of peak annual pumpage ranged from about 260,000 acre-ft/yr (Templin and others, 1995) to about 480,000 acre-ft/yr (California Department of Water Resource, 1980). The pumpage database developed by Templin and others (1995) underestimates the pumpage in the ground-water basin, because it does not include agricultural pumpage estimates for the Kern County part of the study area. Increased pumping costs owing to increased pumping lifts and rising electricity costs resulted in a decline in pumpage beginning in the mid 1950s. In 1972, imported water from northern California became available further reducing the demand for ground water.

Owing to the differences and uncertainties in the previous estimates of pumpage and the incomplete record for the model period (1915–95), annual pumpage was recalculated for this study (fig. 5). The revised estimates, which were calculated using the previous estimates and the new data collected during this study, indicate that pumpage reached a high of 395,000 acre-ft in 1951 and a modern (post 1915) low of 70,600 acre-ft in 1990. Pumpage for the period 1915–51 was based on the estimates of Snyder (1955). Snyder (1955) estimated pumpage for 1924–51 using both annual power-consumption data and crop consumptive-use data for intermittent years. The estimates of pumpage from these data were nearly equal (fig. 5), and were assumed valid for this study. The pumpage for 1952–95 was calculated for this study using irrigated crop acreage data, crop consumptive-use data, and data from the pumpage database created by Templin and others (1995).

Owing to the known limitations in the agricultural component of the pumpage data in the pumpage database created by Templin and others 1995), only the public-supply data from the pumpage database presented by Templin and others (1995) were used for 1952–95 estimates presented in this study. Pumpage for public supply is metered and therefore was assumed to be well documented in the pumpage database. Data compiled from public-supply agencies support this assumption. Pumping of small quantities of ground water for domestic use occurs in the study area, but, because it was not measured, it was not included in estimates of annual pumpage.

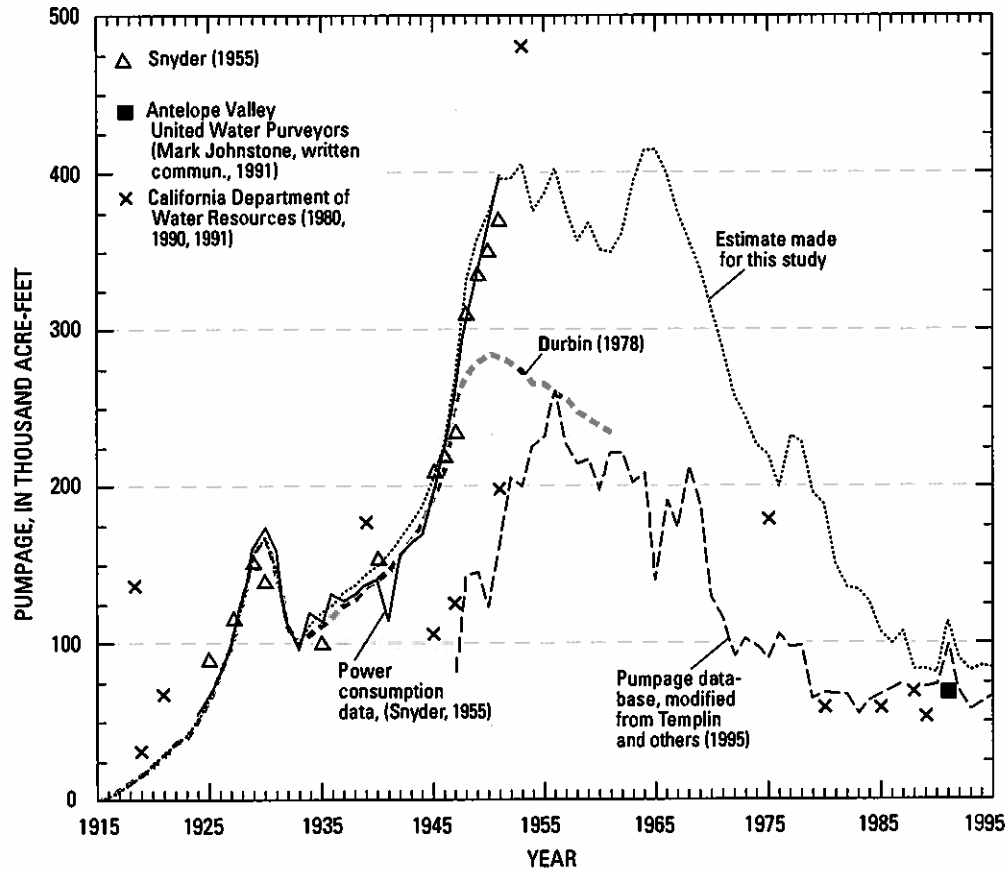

Figure 5. Estimated ground-water pumpage in Antelope Valley, California, 1915–95.

Table 2. Unit consumptive use of crops grown in Antelope Valley, California, 1952–95

[Unit consumptive use in acre-feet per acre; CDPW, California Department of Public Works; CIMIS, California Irrigation Management Information System; UCCE, University of California Cooperative Extension. —, no data]

Crop	Source			
	Snyder (1955)	CDPW (1955)	Templin and others (1995)	CIMIS/ UCCE [1] (1994)
Alfalfa	3.37	3.6	4.3	4.8
Pasture	3.18	3.4	4.3	4.8
Orchard	2.6	2.8	2.6	—
Sugar beets	2.54	2.6	—	—
Field crops	2.1	2.1	2.2	—
Truck crops	1.92	2.0	1.5	—

[1] Reference evapotranspiration (ET_o) × crop coefficient (K_c) [ET_o from California Irrigation Management Information System (CIMIS) (2001) and K_c from University of California Cooperative Extension (1994)].

The agricultural component of annual pumpage for 1952–95 was estimated by calculating the total annual crop consumptive use from irrigated crop acreage data obtained from the Los Angeles County Agricultural Commissioner and unit consumptive-use data for the crops. Unit consumptive use is defined as the quantity of water, in acre-feet, used per acre of crop grown. Published estimates of the unit consumptive use of crops grown in Antelope Valley (table 2) are from the California Department of Public Works (1955), Snyder (1955), and Templin and others (1995). The estimates reported by Templin and others (1995) were from the California Department of Water Resources (CDWR). Estimates also were calculated for the unit consumptive use of alfalfa and pasture (table 2); these estimates were calculated using crop coefficients (University of California Cooperative Extension, 1994) and the reference evapotranspiration rate for Antelope Valley. The reference evapotranspiration rate data are from the California Irrigation Management Information System (CIMIS), a repository of climatological data used for irrigation management and operated by the CDWR.

CIMIS uses local climatological data to determine a reference evapotranspiration rate (ET_0) for unstressed (well-watered) pasture. The unit consumptive use (ET_C) for a given crop is calculated as the product of ET_0 and the crop coefficient (K_C) that relates the evapotranspiration rate of the given crop to a reference crop (pasture). The normal year ET_0 for the ground-water basin was estimated by averaging the normal year ET_0 data for Lancaster and Palmdale obtained from CIMIS. For this study, ground-water pumping for irrigation of alfalfa was assumed to occur only from March through October: the total ET_0 for these months in a normal year is 4.8 ft. The University of California Cooperative Extension (1994) reports that the K_c for alfalfa ranges from 0.4 to 1.2, depending on the stage of growth, but that some researchers recommend using a K_c value of 1.0 for alfalfa. A K_c value of 1.0 was used for this study, which resulted in a unit consumptive use of 4.8 ft, which was the same as that for pasture.

The ET_c values for orchard, sugar beets, and field crops are consistent among the sources shown in table 2. The ET_c values estimated by Snyder (1955) for these crops were used to calculate the annual consumptive use of these crops for 1952–95 so that the values were consistent with those used by Snyder (1955) to estimate agricultural pumpage for 1915–51. Because the estimates of ET_c for alfalfa and pasture are not consistent among the sources shown in table 2, the annual consumptive use for alfalfa and pasture for 1952–95 was calculated using the ET_c values estimated from K_c and ET_0 data. The ET_c for alfalfa and pasture (4.8 acre-ft/acre) was used to calculate annual consumptive use for 1952–95 because these values were based on the most current crop consumptive-use studies. However, annual consumptive-use estimates for alfalfa and pasture were not recalculated for 1915–51 using the current unit consumptive-use values of 4.8 acre-ft/acre because annual crop acreage data were not available for this period.

Annual crop acreage data for 1952–95 are shown in table 3. Onions were assumed to be a field crop and, therefore, the ET_c for field crops reported by Snyder (1955) (table 2) was used to calculate the total annual consumptive use of onions. The total annual crop consumptive use in the study area for 1952–95 (table 3) was calculated using the following equation:

$$CU_T = (A_{alf} \times CU_{alf}) + (A_{past} \times CU_{past}) + (A_{orch} \times CU_{orch}) + (A_{beets} \times CU_{beets}) + (A_{onions} \times CU_{onions}) \tag{1}$$

where

CU_T	is the total annual crop consumptive use $[L^3]$,
A_{alf}	is the area of irrigated alfalfa $[L^2]$,
CU_{alf}	is the unit consumptive use for alfalfa [L],
A_{past}	is the area of irrigated pasture $[L^2]$,
CU_{past}	is the unit consumptive use for pasture [L],
A_{orch}	is the area of irrigated orchards $[L^2]$,
CU_{orch}	is the unit consumptive use for orchards [L],
A_{beets}	is the area of irrigated sugar beets $[L^2]$,
CU_{beets}	is the unit consumptive use for beets [L],
A_{onions}	is the area of irrigated onions $[L^2]$, and
CU_{onions}	is the unit consumptive use for onions [L].

Table 3. Crop area acreage, annual crop consumptive use, and total applied water used for irrigation in the Los Angeles County part of Antelope Valley, California, 1952–95

[Crop area data from Los Angeles County Agricultural Commissioner (1952–95), written commun.]

Year	Crop area, in acres					Total annual crop consumptive use, in thousand acre-feet	Total applied water, in thousand acre-feet
	Alfalfa	Orchard	Pasture	Onions	Beets		
1952	36,000	3,408	4,108	0	0	199.8	285.5
1953	36,400	3,530	4,300	0	0	202.8	289.8
1954	33,200	3,616	4,400	0	0	188.2	268.8
1955	34,800	3,830	4,060	0	0	196.0	280.0
1956	35,900	3,740	4,000	70	0	200.8	286.9
1957	34,000	2,645	3,700	140	0	185.8	265.4
1958	31,800	2,644	3,800	415	0	176.1	251.5
1959	32,600	2,716	3,800	640	0	180.7	258.2
1960	32,500	2,772	1,900	670	0	175.7	250.9
1961	32,000	2,396	1,800	50	435	171.0	244.3
1962	32,000	2,432	1,600	50	2,125	174.9	249.9
1963	36,500	2,470	1,400	90	2,150	196.3	280.5
1964	38,000	2,420	1,700	100	2,660	205.4	293.4
1965	38,000	2,384	2,000	160	1,466	203.1	290.1
1966	36,000	2,385	2,000	170	1,470	193.5	276.5
1967	34,000	2,088	2,000	0	1,660	182.6	260.9
1968	32,000	2,097	1,800	80	1,584	172.5	246.5
1969	30,000	1,838	1,500	0	1,520	160.6	229.4
1970	27,700	1,855	1,500	60	1,500	149.7	213.9
1971	25,400	1,867	1,000	0	1,500	137.3	196.1
1972	22,400	1,591	1,000	80	1,500	121.7	173.9
1973	21,400	1,590	400	240	1,220	115.0	164.3
1974	19,800	1,540	400	250	1,070	106.7	152.4
1975	19,000	1,393	400	700	1,200	103.4	147.8
1976	20,000	1,162	375	1,200	1,868	109.8	156.9
1977	23,000	1,162	375	2,500	3,700	131.6	188.0
1978	23,000	1,180	400	1,700	3,200	128.8	184.0
1979	22,800	1,219	0	1,715	2,200	124.5	177.8
1980	22,500	1,349	100	425	3,860	125.4	179.2
1981	20,000	1,015	100	977	2,775	110.2	157.5
1982	16,200	1,046	100	1,433	340	86.9	124.2
1983	13,757	1,104	200	1,810	317	76.5	109.2
1984	12,176	820	0	1,477	260	66.1	94.5
1985	10,671	852	0	1,580	0	58.6	83.8
1986	8,413	704	0	1,481	0	46.9	67.0
1987	8,895	700	0	1,497	0	49.2	70.3
1988	7,620	700	0	1,702	0	43.5	62.2
1989	6,300	800	0	1,675	0	37.6	53.7
1990	6,211	815	0	1,550	0	37.0	52.8
1991	5,768	705	0	1,690	0	34.6	49.5
1992	5,222	728	0	1,665	0	32.1	45.8
1993	5,532	738	0	1,564	0	33.4	47.7
1994	5,565	830	0	1,346	0	33.5	47.9
1995	5,480	842	0	1,669	0	33.9	48.4

The total water applied for agriculture in the Los Angeles county section of the ground-water basin (table 3) was calculated by dividing total annual crop consumptive use by irrigation efficiency. Irrigation efficiency was assumed to be 70 percent on the basis of previous studies (California Department of Public Works, 1955; Snyder, 1955), a comparison of water application rates (Orloff and others, 1989), and crop consumptive-use rates for alfalfa (University of California Cooperative Extension, 1994). The actual irrigation efficiency likely is spatially and temporally variable and controlled by several factors including irrigation practices and soil characteristics; this variability was not represented in this study. The agricultural component of annual pumpage for 1952–95 was estimated by subtracting imported water, local surface-water diversions, and reclaimed wastewater used for agriculture from the total annual water applied for agriculture.

Records of annual irrigated crop acreage and agricultural pumpage are not available for Kern County and, therefore, estimated agricultural pumpage for that part of the study area was based on the relation between land use and ground-water use for 1961 and 1987. Land-use maps and agricultural pumpage data for Los Angeles County were used to estimate the quantity of ground-water pumpage per acre of agricultural land in 1961 and 1987. This ratio of pumpage per acre of agricultural land was then applied to agricultural land-use data for Kern County to estimate agricultural pumpage for the Kern County part of the study area for those years. In both 1961 and 1987, agricultural pumpage in the Kern County part of the study area was about 18 percent of the annual agricultural pumpage in the Los Angeles County part of the study area. This relation was assumed constant for the period 1952–95.

The spatial distribution of pumpage in the study area changed as agriculture declined in the late 1960s and 1970s and as urban areas grew in the 1980s. Data from the pumpage database were used to show changes in the spatial distribution of pumpage in the ground-water basin. Although the agricultural component of the pumpage database is known to be incomplete, it was assumed that the spatial distribution of pumpage in the database is representative of the spatial distribution of actual pumpage in the basin. Prior to the 1980s, ground water was pumped primarily for agricultural use and mainly in the western and eastern parts of the Lancaster subbasin (fig. 6*A*). Since the 1980s, much of the pumpage has been for urban use, and the pumping centers have shifted from agricultural areas to urban areas near Rosamond, Edwards Air Force Base, Lancaster, and Palmdale (fig. 6*B*).

Natural discharge from evapotranspiration is greatly affected by changes in water levels caused by ground-water pumping. The water table has declined to a depth at which natural discharge from evapotranspiration is minimal. As with natural recharge, natural discharge as ground-water underflow is affected by changes in water-level gradients, but ground-water underflow is only a small component of the overall water budget for the basin.

Ground-Water Levels and Movement

Prior to ground-water development, the depth to water in the Lancaster subbasin was less than or equal to 50 ft below land surface in most of the subbasin, and, in the areas around the playas, artesian conditions existed. In the western part of the Lancaster subbasin and in the southern part near Palmdale, the depth to water was about 200 ft below land surface. Data on the depth to water in the Buttes, Finger Buttes, Neenach, Pearland, and West Antelope subbasins are limited, especially for the upslope parts of the these subbasins. Available data indicate that the depth to water in these subbasins ranged from about 50 ft below land surface in the lower part of the Neenach subbasin to about 200 ft below land surface in the higher parts of the Buttes, Pearland, and Finger Buttes subbasins. In the North Muroc subbasin, depths to water ranged from 50 to 100 ft below land surface. Water-level altitudes were highest in the Finger Buttes (3,300 ft above sea level) and Pearland (3,200 ft above sea level) subbasins (fig. 4) and lowest around the playas in the northeast part of the Lancaster subbasin (2,300 ft above sea level) and in the North Muroc subbasin (2,200 ft above sea level) (fig. 4). Around the playas, water levels were near land surface, and ground water was discharged in these areas largely by evapotranspiration and springs.

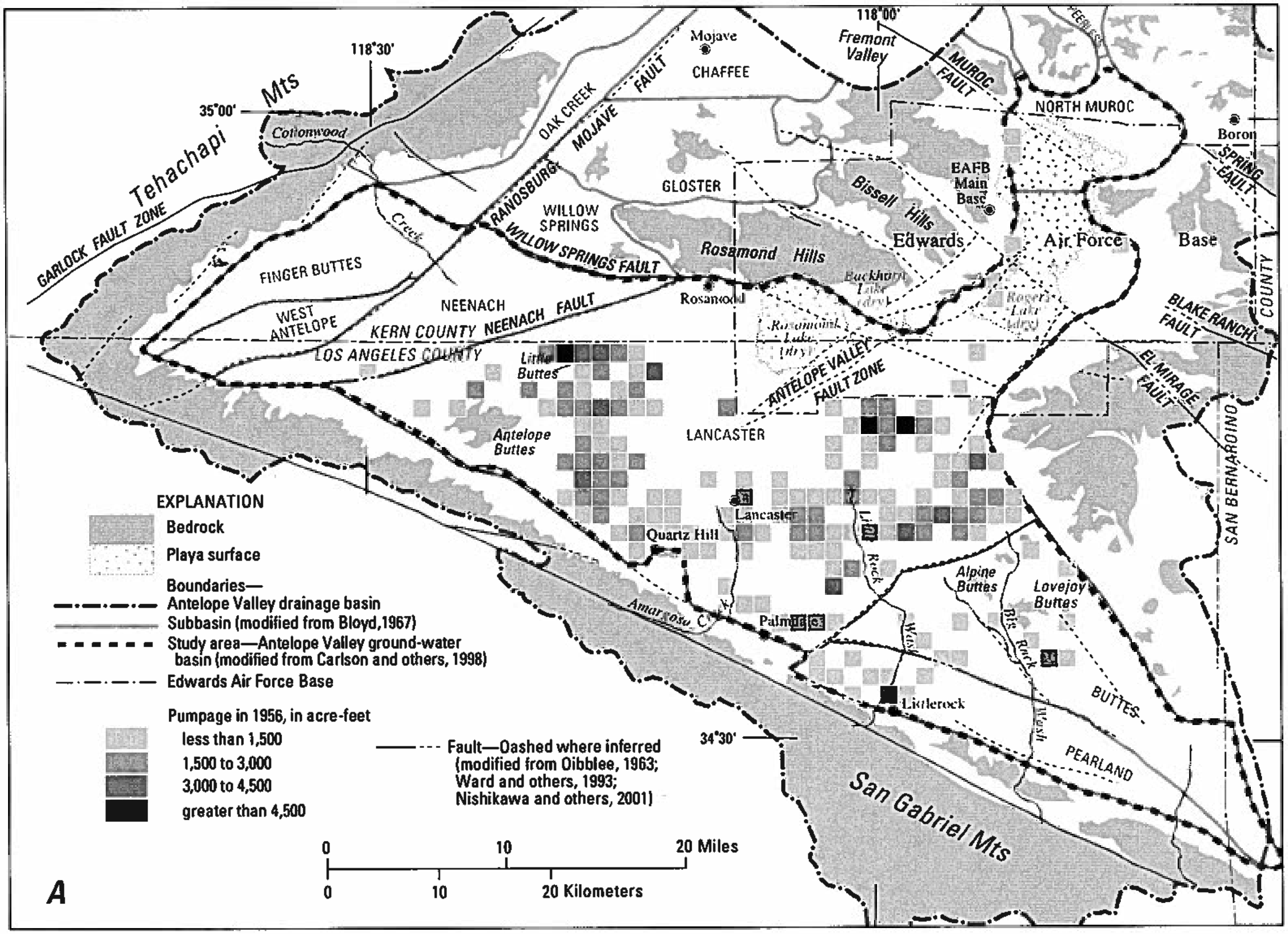

Figure 6. Distribution of pumpage in Antelope Valley, California. ***A***, 1956; ***B***, 1995.

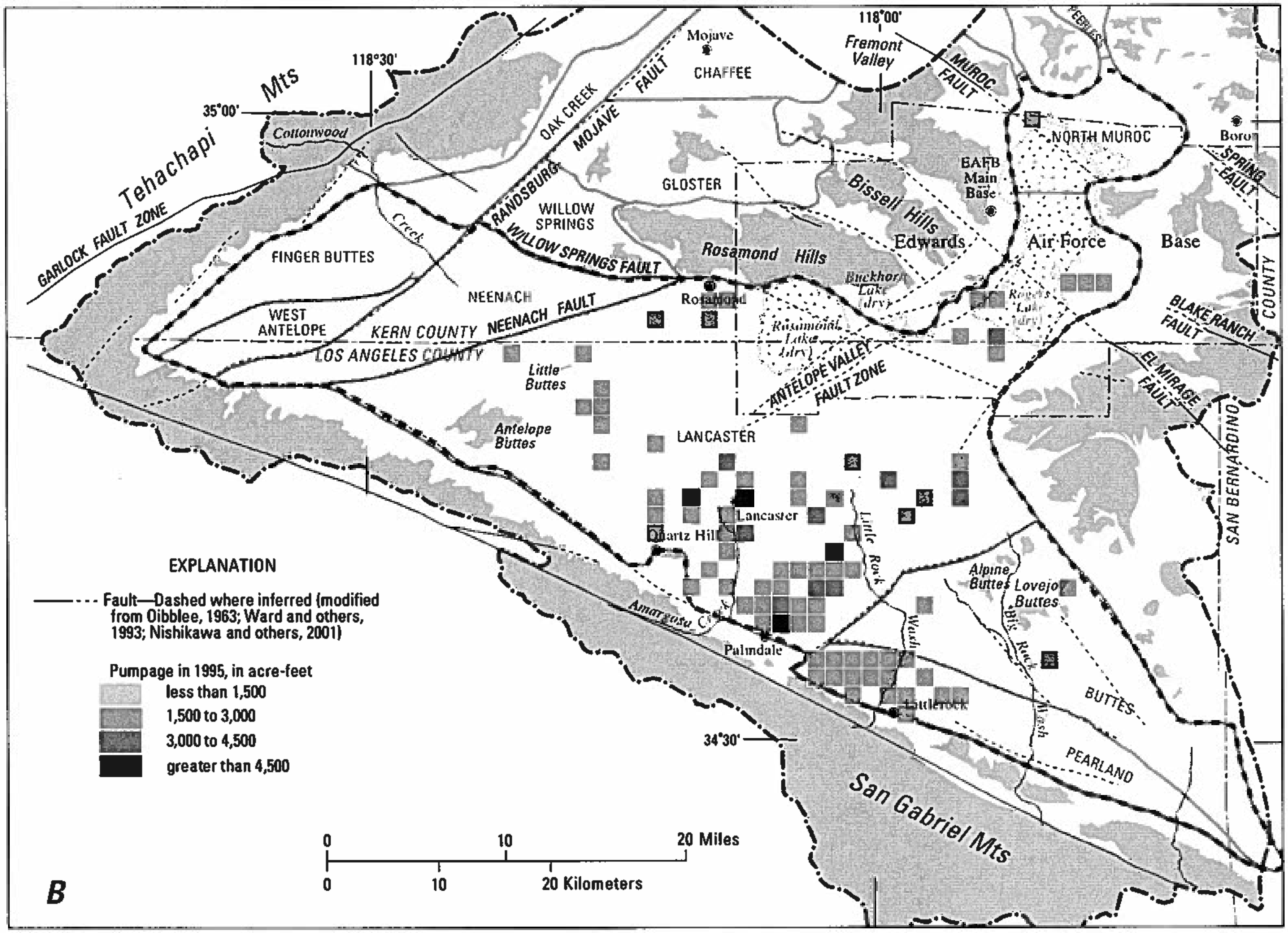

Figure 6.—Continued.

Ground water moves from areas of high water-level altitudes to areas of low water-level altitudes; therefore, the general direction of ground-water flow can be inferred from contours of water level. Ground water flowed from areas of recharge along the mountain fronts and stream channels toward areas of discharge around Rosamond, Buckhorn, and Rogers Lakes (dry) (fig. 4). In the Finger Buttes and West Antelope subbasins, ground water generally moved from northwest to southeast. In the Neenach subbasin, ground water generally moved from west to east. In the Buttes and Pearland subbasins, ground water generally moved from southeast to northwest. In the Lancaster subbasin, ground water moved from the upslope areas in the southwestern, southern, and southeastern parts of the subbasin to the discharge areas in the northern and northeastern part of the subbasin. In the North Muroc subbasin, there was a small water-level gradient toward the north where some ground water flowed into the Fremont Valley Basin.

Since the 1920s, ground-water use has exceeded estimated natural recharge. This overdraft has caused water levels to decline by more than 200 ft in some areas and by at least 100 ft in most of the study area. In agricultural areas, declining water levels began to level off in the late 1970s and, in some areas, water levels began to rise. Since 1983, water levels have risen by as much as 45 ft in areas where land use is predominately agriculture (Carlson and others, 1998). In urban areas, water levels have continued to decline.

Water-level data collected in spring 1996 (Carlson and others, 1998) represent regional water levels after more than 75 years of ground-water development in the basin (fig. 7). In the Lancaster subbasin, depth to water is more than 100 ft below land surface throughout most of the subbasin and the water table has declined to a level that has eliminated the discharge of ground water by evapotranspiration. In the eastern and western parts of the subbasin where most of the agricultural pumping has occurred, depth to water is more than 200 ft below land surface; in some areas, depth to water is more than 300 ft below land surface. In the area around Palmdale, where most of the pumping for public supply has occurred, depth to water is more than 500 ft below land surface. In the Finger Buttes, Neenach, and West Antelope subbasins, depth to water ranges from about 150 ft to more than 350 ft below land surface. In the Buttes and Pearland subbasins, depth to water ranges from about 50 ft to about 250 ft below land surface, and in the North Muroc subbasin, depth to water ranges from about 100 ft to near 200 ft below land surface. Water-level altitudes are highest in the Neenach (2,800 ft above sea level) Pearland (2,800 ft above sea level) and Finger Buttes subbasins (data from a single data point in the Finger Buttes subbasin suggest that the water-level altitudes in this subbasin may be about 3,200 ft above sea level) (Carlson and others, 1998). The lowest water-level altitude is in the Lancaster subbasin in the area around Palmdale (2,050 ft above sea level) (fig. 7).

In the Neenach subbasin, ground water now moves to the northeast and flows into the Lancaster subbasin. In the Buttes and Pearland subbasins, ground water generally continues to move southeast to northwest. In the Lancaster subbasin, ground water flows from areas of natural recharge toward areas of low water-level altitude in the south-central part of this subbasin (fig. 7). Although not evident from the contours shown on figure 7, there also is an area of low water-level altitude centered near the primary production wells at Edwards Air Force Base, near the south end of Rogers Lake (Carlson and others, 1998); ground water flows from the boundary between the Lancaster and North Muroc subbasin toward this ground-water low (Rewis, 1995). An area of high water-level altitude exists in the central part of the Lancaster subbasin southwest of Rosamond Lake (fig. 7); the high water levels may be the result of limited agricultural pumping and low-permeability alluvial material in this area. Because pumping for agriculture has been limited, little drawdown has occurred over time. Recharge from the infiltration of wastewater from the Lancaster Water Reclamation Plant discharged to ponds in the area also may be contributing to the high water-level altitudes. In the North Muroc subbasin, the water-level gradient is fairly flat, but a small amount of water may continue to flow toward the Fremont Valley Basin from the North Muroc subbasin.

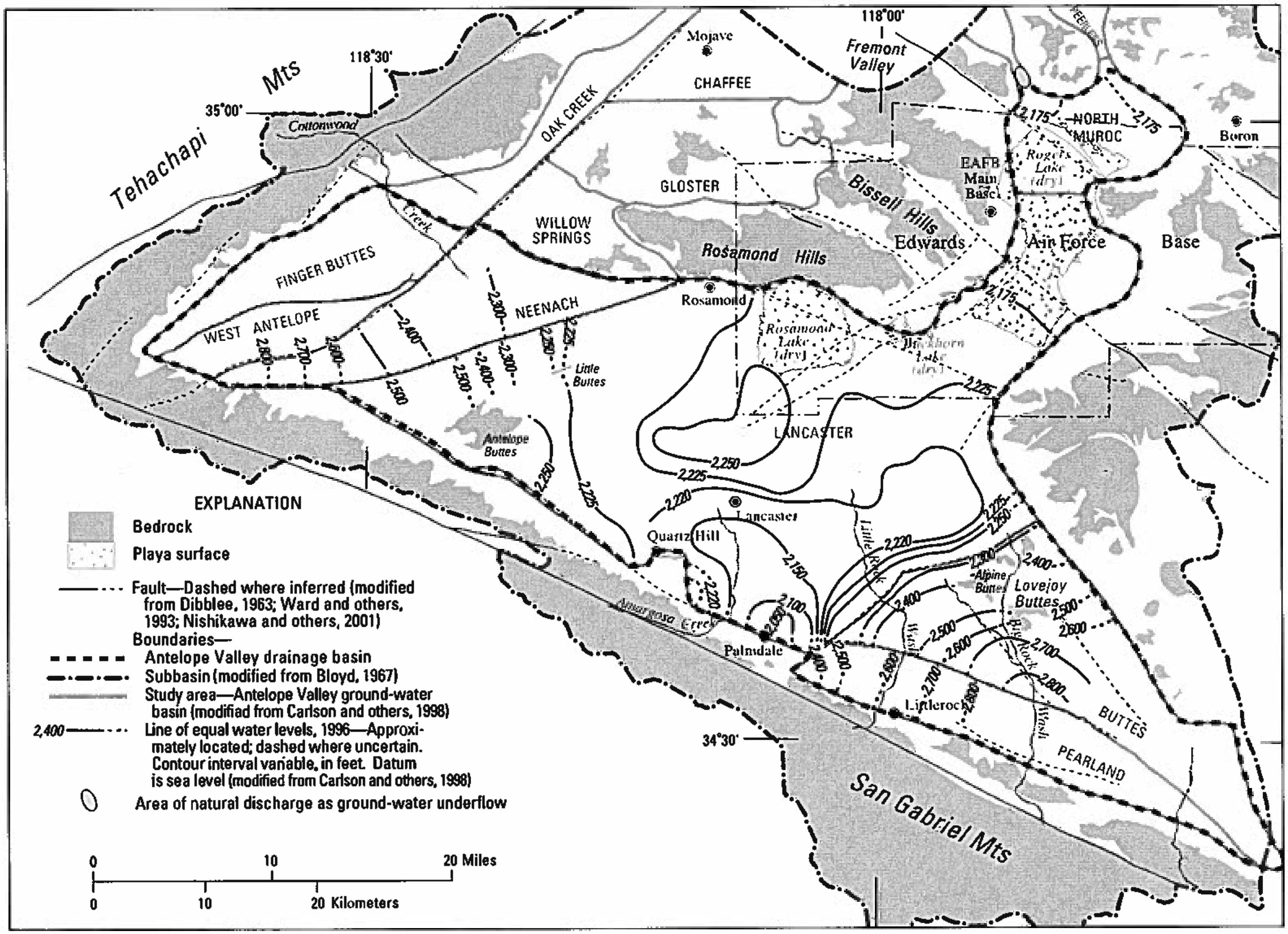

Figure 7. Ground-water levels in spring 1996 and location of area of natural discharge as ground-water underflow in the Antelope Valley ground-water basin, California.

LAND SUBSIDENCE AND AQUIFER-SYSTEM COMPACTION

Land subsidence is the gradual settling or sudden sinking of the Earth's surface owing to subsurface movement of earth materials. One of the principal causes of land subsidence is the gradual compaction of susceptible aquifer systems that can accompany ground-water level declines caused by ground-water pumping (Galloway and others, 1999). Results of Global Positioning System and spirit leveling surveys indicate that as much as 6.6 ft of subsidence occurred in the valley between 1930 and 1992 (fig. 8) (Ikehara and Phillips, 1994). The spatial variability in the amount of land subsidence in Antelope Valley is affected by the magnitude of water-level declines and the distribution of compressible sediments. The large amount of subsidence measured around bench marks BM 474 and BM 1171A and between Little Buttes and Rosamond (fig. 8) is the result of water-level declines coupled with a significant thickness of compressible sediments in the aquifer system. No measurable land subsidence was detected near Palmdale, although it is an area of large water-level declines (Carlson and others, 1998). The lack of subsidence in this area indicates that compressible sediments may not exist or water levels may not have declined to the level at which inelastic (permanent) compaction of the sediments would occur. The results of a more recent study, which used satellite-based interferometric synthetic aperture radar (InSAR) to measure land subsidence during the period October 20, 1993, to December 22, 1995, indicated that locally, more than 0.16 ft of subsidence occurred and likely is still occurring in the valley (Galloway and others, 1998). Detrimental effects of land subsidence include the loss of aquifer storage, increased flooding, cracks and fissures at land surface, damage to man-made structures, and intangible economic costs.

Compaction of the aquifer system occurs when the hydraulic head or fluid pressure in compressible, fine-grained sediments declines, releasing porewater in the compressible sediments from storage (Fluid pressure has units of stress and is equal to hydraulic head times the specific weight of water). For a constant total stress on the aquifer system the associated decrease in fluid pressure is accompanied by an equivalent increase in the effective or intergranular stress on the granular matrix or skeleton of the aquifer system, resulting in aquifer-system compaction. The magnitude of the compaction is governed by the compressibility of the sediments which varies by an order of magnitude or more depending on whether the intergranular stress changes are in the elastic or inelastic range of stress for the compacting sediments. Elastic compaction is compaction that occurs when the skeletal structure of the sediments is not permanently rearranged: it can be reversed by an associated rise in hydraulic head. Inelastic compaction is compaction that occurs when there is a permanent rearrangement of the skeletal structure of the sedimentary matrix; it cannot be reversed by a rise in hydraulic head, and, therefore, results in a permanent lowering of land surface and a loss of ground-water storage capacity. The point to which hydraulic heads must decline to cause inelastic compaction in the compressible sediments is termed the preconsolidation head. When hydraulic head in the compressible sediments declines below the existing preconsolidation head, permanent compaction can occur and a new lower preconsolidation head is established. When heads fluctuate above the preconsolidation head, generally small magnitude elastic (reversible) compaction occurs. Detailed discussions of the mechanics of compaction and its relation to land subsidence are given in reports by Leake and Prudic (1991), Ikehara and Phillips (1994), Galloway and others (1998), and Galloway and others (1999).

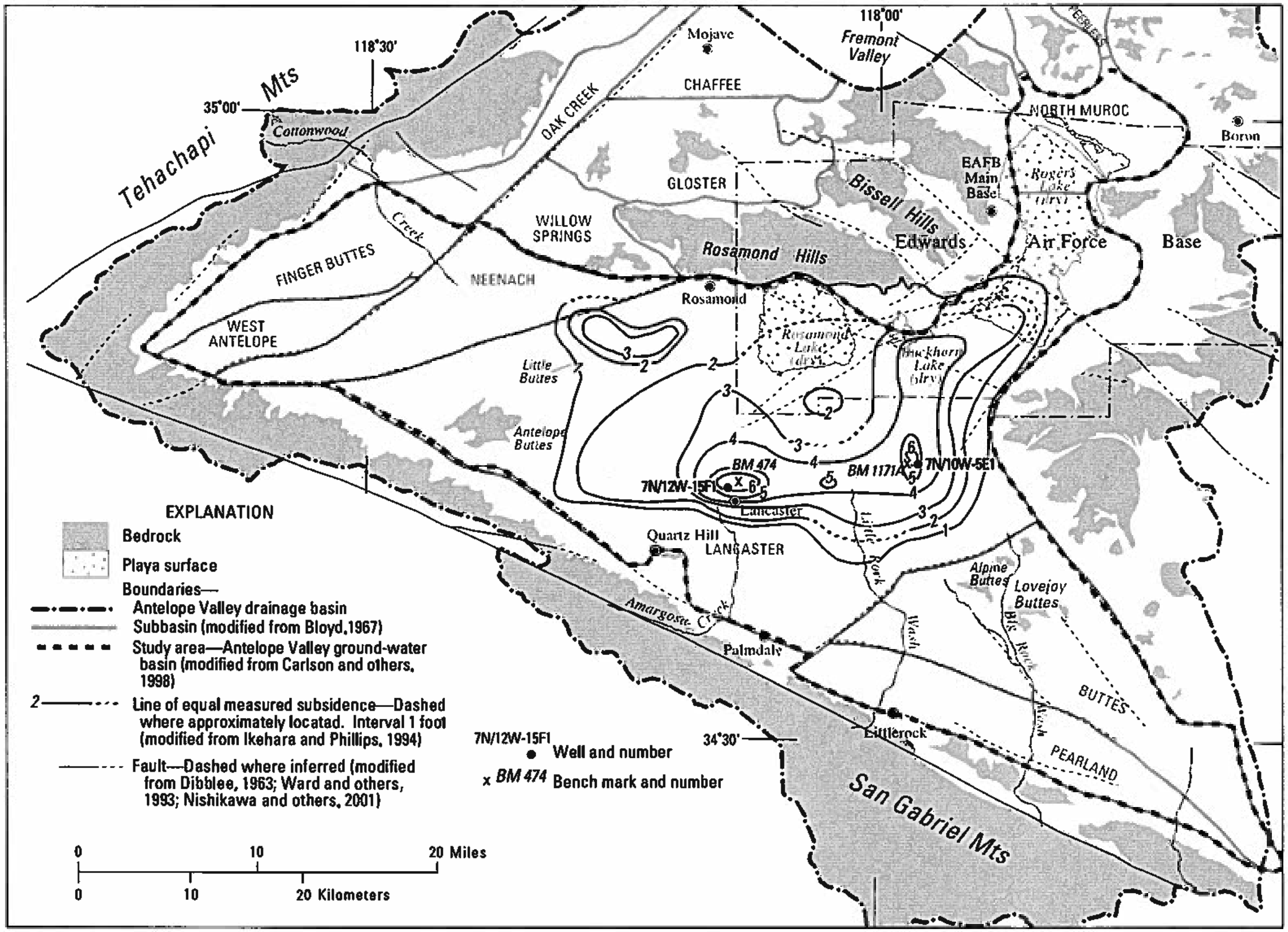

Figure 8. Measured subsidence in the Antelope Valley ground-water basin, California, 1930–92.

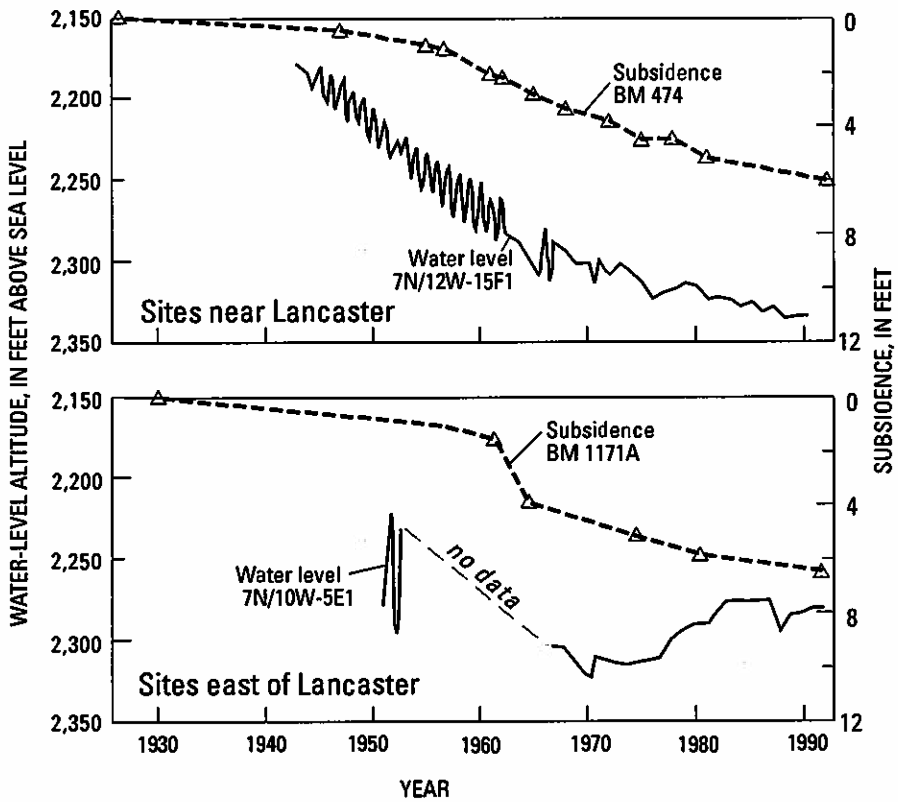

Figure 9. Paired water-level and land-subsidence data for sites near and east of Lancaster, Antelope Valley, California (modified from Ikehara and Phillips, 1994). Location of bench marks and wells are shown on figure 8.

As noted earlier, the ground-water system in Antelope Valley is made up of alluvial and lacustrine sedimentary deposits. The alluvial deposits consist of sand and gravel interbedded with thin, fine-grained silt and clay layers. The lacustrine deposits consist of thick clay layers interbedded with thin coarse-grained material. Compaction can occur in both the thin and the thick fine-grained silt and clay layers that form confining beds, or aquitards; little compaction, however, can occur in the sand and gravel deposits. As described by Freeze and Cherry (1979), "... the term aquitard has been coined to describe the less-permeable beds in a stratigraphic sequence. These beds may be permeable enough to transmit water in quantities that are significant in the study of regional ground-water flow, but their permeability is not sufficient to allow the completion of production wells within them." The thickness of the aquitards affects the rate and the duration of aquifer-system compaction. The thickness of the aquitard affects the rate at which the fluid pressure of the aquitard equilibrates with the fluid pressure of the surrounding coarse-grained material; thin aquitards equilibrate faster than thick aquitards. Hydraulic heads in aquifer material surrounding the thick aquitards may recover to levels higher than preconsolidation head, but compaction can continue to occur until the hydraulic heads in the thick aquitards equilibrate with hydraulic heads in the surrounding coarse-grained deposits. This equilibration can take years to complete and is termed residual compaction. The fluid-pressure equilibration between thick or thin aquitards and the surrounding aquifer results in release from or uptake to storage in the aquitards and involves fluid-flow between the aquitards and aquifer. This flow is primarily vertical as the lateral extent of aquitards is generally much greater than their thickness.

The relation between hydraulic head, which is measured as water levels in wells, and compaction, which is typically measured as land subsidence at land surface, can be seen in figure 9. The measured land subsidence at BM 474 near Lancaster is directly related to the continuous water-level decline measured in nearby well 7N/12W-15F1. The measured land subsidence at BM 1171A east of Lancaster is related to the water-level decline measured in nearby well 7N/10W-5E1 from about 1950–70, however the continued measured land subsidence from 1970s to the early 1990s does not correspond to the measured water-level recovery in the nearby well during this same time period. The subsidence that occurred at BM 1171A from the 1970s to the early 1990s may be the result of residual compaction.

SIMULATION OF GROUND-WATER FLOW

The objective of constructing a numerical ground-water flow model of the Antelope Valley ground-water basin was to gain a better understanding of the aquifer system and to develop a tool for evaluating and predicting aquifer responses to various water-management alternatives. Because land subsidence has been occurring in the Antelope Valley since the 1930s (Ikehara and Phillips, 1994; Galloway and others, 1998), a significant amount of the water being pumped in the valley may come from the compacting sediments. It is important, therefore, that a model of the valley have the capability to simulate compaction. Results of aquifer-system compaction simulations can be used to evaluate the potential for future compaction and land subsidence due to water-level declines in the valley.

The numerical model used for this study is the USGS modular three-dimensional finite-difference ground-water flow model (MODFLOW) (McDonald and Harbaugh, 1988). The basic MODFLOW code was used with the Interbed Storage 1 (IBS1) Package (Leake and Prudic, 1991) to simulate aquifer-system compaction and land subsidence and the Horizontal Flow Barrier (HFB) Package (Hsieh and Freckleton, 1993) to simulate the effect of horizontal barriers, such as faults, to ground-water flow. Ground-water levels were calculated at discrete points by solving simultaneous equations that approximate the partial differential equation for ground-water flow. The discrete points are the result of discretization of the model area into a series of layered rectangular model cells with the points (or nodes) located at the center of model cells. Land subsidence is computed at a model cell by summing the compaction simulated in each of the model layers, and is reported for the model cell in the uppermost layer.

The model can simulate ground-water levels and fluxes and aquifer-system compaction on the basis of the ability of the aquifer system to transmit water (transmissivity), its capacity to store and release water (storage coefficient), and the applied hydrologic stresses (recharge and discharge). The model, however, is only an approximation of the aquifer system being simulated and, therefore, cannot exactly duplicate or represent the actual system. Because model development requires the use of data, assumptions, and simplifications to approximate the system, the model is only as accurate as the assumptions and data used to develop the model.

Model Discretization and Boundaries

The model grid consists of 43 rows and 60 columns with a total of 2,580 square cells (fig. 10). Each cell represents 1 mi^2 with a distance of 5,280 ft (1 mi) on a side. The aquifer system was discretized vertically into three layers. Layer 1 represents the upper aquifer and is unconfined throughout most of the ground-water basin. Around the southern part of Rogers Lake and west to Rosamond Lake, where surface clays act as a confining unit for the aquifer, layer 1 was simulated as confined or unconfined, depending on the water level. Where layer 1 is unconfined, the upper boundary of the layer is the water table. Where layer 1 is confined, the upper boundary of the layer is the bottom of the confining clay, which is 61 to 285 ft below land surface. The lower boundary of layer 1 is at an altitude of 1,950 ft above sea level. Layer 2 is confined and represents the middle aquifer, which extends from 1,950 to 1,550 ft above sea level. Layer 3 is confined and represents the lower aquifer, which extends from 1,550 to 1,000 ft above sea level. Layers 1, 2, and 3 have 921, 626, and 536 active model cells, respectively. The lacustrine deposits in each aquifer are included in the layers representing the aquifers. Alluvial material at depths below 1,000 ft above sea level was assumed to be well-indurated, impermeable, and not a significant part of the regional flow system. Where the altitude of bedrock is above the defined layer bottom, the layer bottom is equal to the altitude of bedrock. The model grid and the lateral boundaries of the model layers are shown in figure 10.

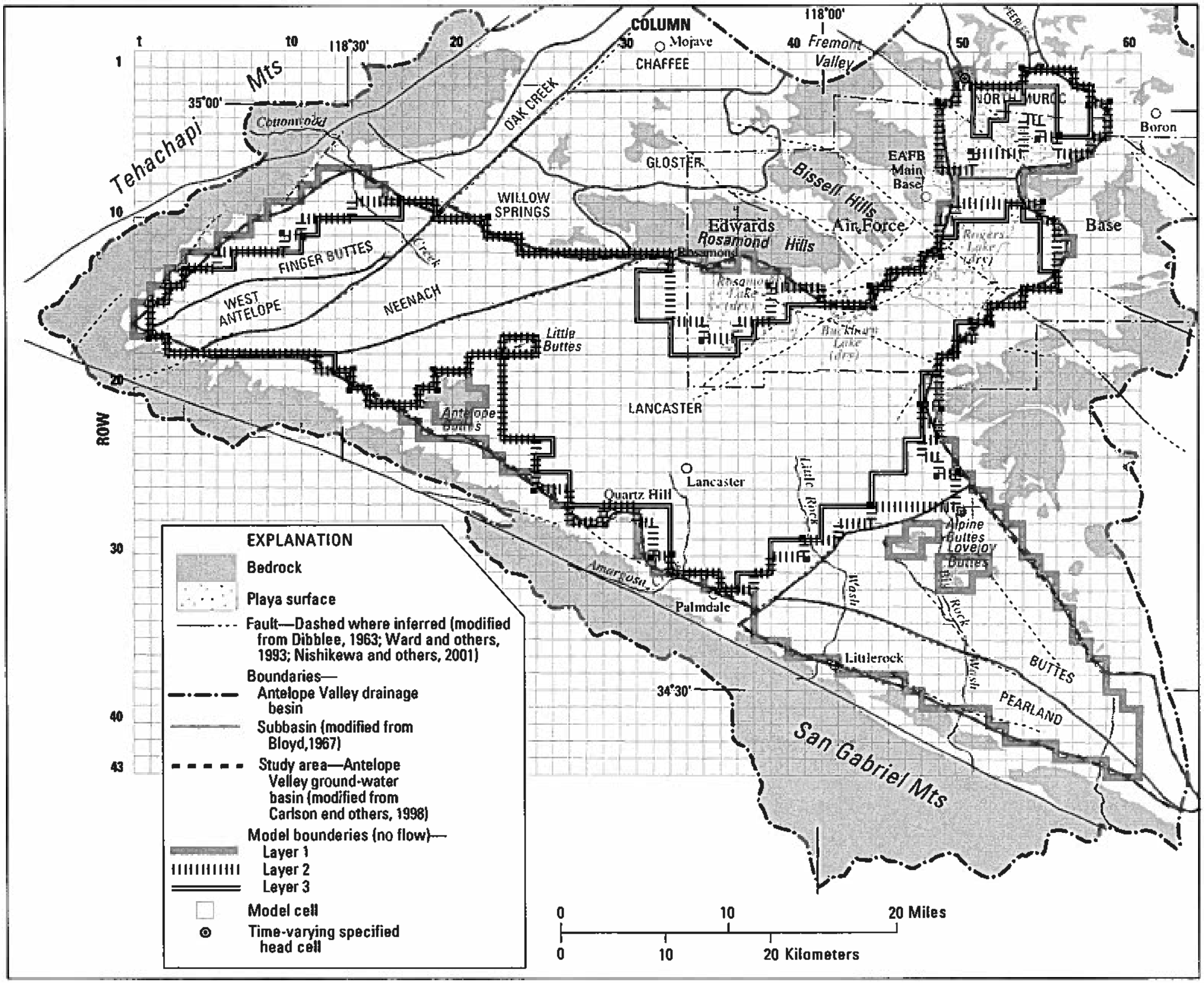

Figure 10. Model grid and boundaries of model layers in the ground-water flow model of the Antelope Valley ground-water basin, California.

Temporally, the model was discretized into 81 stress periods, each 1 year in length, in which specified stresses were held constant. These 1-year periods were selected to correspond to the intervals when ground-water pumpage was reported and water levels in wells in the monitoring network were measured. Water levels and aquifer-system compaction in each active model cell were output from the model at the end of each stress period.

Except for the area around Rogers Lake where layer 1 may be confined by clay, the upper boundary of the model is the water table. It was simulated as a free-surface boundary that was allowed to move vertically in response to imbalances in the inflows and outflows to the model. The lateral boundaries of the model are all no-flow boundaries, except one boundary cell representing the area north of Rogers Lake where ground water discharges into the Fremont Valley. No water enters or leaves the system at the no-flow boundaries. These lateral boundaries are located at the contact between the aquifer and bedrock or barrier faults. To simulate discharge into Fremont Valley, the model cell for layer 1 for this location was designated as a time-varying specified-head boundary (fig. 10) where water can enter or leave the system as determined by the water-level gradient between this cell and adjacent active cells. The specified head in this cell was varied for each stress period on the basis of water-level data from nearby wells (Nishikawa and others, 2001). The lower boundary of the model also is a no-flow boundary. This no-flow boundary is located where the aquifer comes into contact with bedrock or at an altitude of1,000 ft above sea level, below which the deposits were assumed to be non-water-bearing.

Model Parameters

Simulation of ground-water flow and fluxes and aquifer-system compaction requires specifying aquifer-system properties and stresses. Aquifer-system properties can vary considerably both horizontally and vertically and thus cannot be precisely represented in a numerical model. The aquifer-system properties specified for each active cell in the model are estimates of the average conditions in the area represented by the cell. Similarly, stresses applied to the system (recharge and discharge) are estimates for the area represented by each cell. The initial aquifer-system properties, with the exception of the storage coefficients for confined aquifers specified for layers 1 and 2, were obtained from the Durbin (1978) model. Recharge and pumpage were estimated as described in earlier sections of this report. Selected properties and stresses were modified within reasonable limits during model calibration: the modifications were made on the basis of recently collected hydrologic data and parameters used in the ground-water flow models of the Edwards Air Force Base area (Sneed and Galloway, 2000; Nishikawa and others, 2001).

Hydraulic Conductivity and Transmissivity

Ground-water flow within the model layers was assumed to be horizontal. Hydraulic conductivity and transmissivity are properties that, in conjunction with the horizontal hydraulic gradient, control horizontal flow of ground water. Hydraulic conductivity is a measure of the water transmitting properties of aquifer material; coarse and (or) well-sorted material have a higher hydraulic conductivity than fine and (or) poorly sorted material. Transmissivity is the product of hydraulic conductivity and saturated thickness and represents the water-transmitting properties of the saturated section of the aquifer. Hydraulic conductivity was specified for layer 1 and transmissivity was specified for layers 2 and 3, because layer 1 is unconfined throughout most of the basin and layers 2 and 3 are confined. Hydraulic conductivity was specified for layer 1 to allow the model to compute changes in the transmissivity as the saturated thickness changes in the aquifer.

Total aquifer-system transmissivity (the combined transmissivities represented by model layers 1–3, in feet squared per day) was estimated from specific-capacity data by multiplying the specific capacity (in gallons per minute per foot of drawdown) by a conversion factor of 230 (Thomasson and others, 1960). The specific-capacity data used to calculate transmissivity for this current study were from Bloyd (1967) and from more recent data from wells owned by the Los Angeles County Department of Public Works (James Hong, Los Angeles County Department of Public Works, Waterworks and Sewer Maintenance Division, written commun., 1997). The current estimates of transmissivity were consistent with those used in the Durbin (1978) model, which were obtained using data from Bloyd (1967). Transmissivities estimated from specific-capacity data probably are only approximations of the total transmissivity of the aquifer system because the wells from which the specific-capacity data were obtained were not perforated over the entire thickness of the aquifer system.

The initial transmissivity of layer 2 was calculated as the product of the saturated thickness (400 ft, except where bedrock is higher than 1,550 ft above sea level) and a hydraulic conductivity of 10 ft/d. The initial transmissivity of layer 3 was calculated as the product of the saturated thickness (550 ft, except where bedrock is higher than 1,000 ft above sea level) and a hydraulic conductivity of 2 ft/d. The hydraulic-conductivity values used for layers 2 and 3 were based on values from the Edwards Air Force Base model (Nishikawa and others, 2001) and on the preliminary results of modeling of the southern part of the Lancaster subbasin (Phillips and others, in press). The initial transmissivity of layer 1 was calculated by subtracting the sum of the initial transmissivities for layers 2 and 3 from the total transmissivity calculated from the specific-capacity data. The initial hydraulic conductivity for layer 1 was then calculated by dividing the initial layer 1 transmissivity by the pre-development saturated thickness of layer 1, which was estimated using water-level estimates from Durbin (1978) (fig. 4). To avoid unreasonably low values of hydraulic conductivity in layer 1, a minimum hydraulic-conductivity value of 2 ft/d was specified for the cells in that layer. The transmissivity of layers 2 and 3 remained constant throughout the entire simulation period because the water table never declined below the top of layer 2. Initial hydraulic-conductivity and transmissivity values for the area around Rogers Lake were modified to generally agree with the values used in a three-dimensional model developed by for the Edwards Air Force Base area (Nishikawa and others, 2001).

Vertical Leakance

Ground-water flow between model layers was assumed to be vertical and to occur when there is a difference in hydraulic head between layers. The vertical conductance between layers, which represents the ability of the aquifer to transmit water vertically, is calculated by the model using a specified vertical leakance value and the cell dimensions. The vertical leakance between model cells, which is a function of cell thickness and vertical hydraulic conductivity, was calculated outside the model using the following equation from McDonald and Harbaugh (1988):

$$\lambda_{k+1/2} = \frac{1}{\dfrac{\Delta z_k /2}{Kz_k} + \dfrac{\Delta z_{k+1}/2}{Kz_{k+1}}}, \qquad (2)$$

where

$\lambda_{k+1/2}$	is the vertical leakance between layers k and k+1 [t^{-1}],
Δz_k	is the thickness of layer k [L],
Δz_{k+1}	is the thickness of layer k+1 [L],
Kz_k	is the vertical hydraulic conductivity of layer k [Lt^{-1}], and
Kz_{k+1}	is the vertical hydraulic conductivity of layer k+1 [Lt^{-1}].

Equation 2 strongly weights the smaller of the two vertical hydraulic conductivity values. For example, if one layer contains thick lacustrine deposits of silt and clay and the other layer contains mostly alluvial deposits of sand and gravel, the vertical leakance between the layers is dependant mostly on the vertical hydraulic conductivity of the lacustrine deposits. The vertical hydraulic conductivities of layers 1, 2, and 3 were assumed to be one-hundreth of the horizontal hydraulic conductivities in areas where the lacustrine deposits are not present between the centers of adjacent layers. Where lacustrine deposits are present in a layer, the vertical hydraulic conductivity of the lacustrine deposits was used for that layer. An estimate of 1.0×10^{-2} ft/d was used for the vertical hydraulic conductivity of the lacustrine deposits, which is consistent with the value used by Durbin (1978) and three orders of magnitude higher than the value used by Nishikawa and others (2001).

Storage Coefficient

The storage (specific yield or storage coefficient) of water-bearing material is the quantity of water released from storage per unit area per unit decline in hydraulic head. The water released from storage is derived from the compression of the granular matrix (skeleton) of the aquifer system and the expansion of fluid. In confined and unconfined aquifer systems the release of water from storage in low-permeability, unconsolidated fine-grained sediments is accompanied by some degree of compression of the fine-grained sediments. The relation between changes in head, expressed as an equivalent change in pore-fluid pressure, and compression of the aquifer system is based on the principle of effective stress first proposed by Terzaghi (1925) for one-dimensional vertical consolidation of saturated sediment,

$$\sigma_e = \sigma_T - p, \tag{3}$$

where effective or intergranular stress (σ_e) is the difference between the total stress (σ_T) and the pore-fluid pressure (p). Under this principle, when the total stress remains constant, a change in pore-fluid pressure causes an equivalent change in effective stress within the aquifer system, which causes the aquifer system to expand or compress under the new load. In aquifer systems, conditions that cause changes in the total stress include the erosion or aggradation of sediment at land surface, or more commonly a change in the position of the water table overlying confined aquifers. For purposes of this discussion, the total stress is assumed constant.

When the effective stress is decreased by an increase in pore-fluid pressure, the aquifer system expands elastically. When the effective stress is increased by a reduction in pore-fluid pressure and the effective stress does not exceed the maximum past effective stress, the aquifer system compresses elastically. When a reduction in pore-fluid pressure causes an increase in effective stress that exceeds the previous maximum effective stress, the pore structure of the fine-grained sediments (aquitards) in the aquifer system undergoes significant rearrangement, resulting in permanent (inelastic) rearrangement of the granular structure, a reduction in pore volume and permanent compaction of the aquitards.

The elastic and inelastic skeletal compressibilities, α'_k, of the aquitards are expressed in terms of the skeletal specific storages, S'_{sk},

$$\begin{aligned} S'_{sk} &= S'_{ske} = \alpha'_{ke}pg, \ \sigma_e \leq \sigma_e(\max), \\ S'_{sk} &= S'_{skv} = \alpha'_{kv}pg, \ \sigma_e > \sigma_e(\max), \end{aligned} \tag{4}$$

where the primes denote aquitard properties, the subscript k refers to the skeletal component of specific storage, or compressibility, subscripts e and v refer to the elastic and virgin (inelastic) properties, p, is fluid density, and g is gravitational acceleration. For a change in effective stress, the aquitard deforms elastically when the effective stress is less than the previous maximum effective stress, $\sigma_e(\max)$; when the effective stress is greater than $\sigma_e(\max)$, the aquitard deforms inelastically. The previous maximum stress is termed the preconsolidation stress or, expressed as an equivalent hydraulic head is termed the preconsolidation head.

In typical aquifer systems composed of unconsolidated to semi-consolidated Cenozoic sediments, S'_{skv} is generally 30 to several hundred times larger than S'_{ske} (Ireland and others, 1984). The product of the elastic or inelastic skeletal specific storage and the aggregate thickness of the aquitards, $\sum b'$, is the aquitard skeletal storage coefficient S'_k:

$$\begin{aligned} S'_k &= S'_{ke} = S'_{ske}\,(\textstyle\sum b'), \quad \sigma_e \leq \sigma_e(\max), \\ S'_k &= S'_{kv} = S'_{skv}\,(\textstyle\sum b'), \quad \sigma_e > \sigma_e(\max), \end{aligned} \tag{5}$$

for the elastic (S'_{ke}) and inelastic (S'_{kv}) range of skeletal compressibility, respectively. A similar set of equations, one for the coarse-grained aquifers and one for pore water, relates the compressibility of the aquifer skeleton (α_k) to the aquifer skeletal storage coefficient (S_k) and the compressibility of water (β_w) to the component of aquifer-system storage attributed to the pore water (S_w):

$$S_k = S_{sk}\,(\textstyle\sum b) = \alpha_k pg(\textstyle\sum b), \tag{6}$$

$$S_w = \beta_w pg[n(\textstyle\sum b) + n'\,(\textstyle\sum b')], \tag{7}$$

where $\sum b$ is the aggregate thickness of the aquifers and n and n' are the porosities of the aquifers and aquitards, respectively. For coarse-grained aquifers interbedded with compressible aquitards, the difference between the elastic and inelastic compressibilities of the aquifer skeleton is considered relatively insignificant, and $\alpha_k \cong \alpha_{ke}$.

The aquifer-system storage coefficient S is defined as the sum of the skeletal storage coefficients of the aquitards and aquifers (equations 5–6) plus the storage attributed to water compressibility (equation 7). Thus,

$$S = S'_k + S_k + S_w. \qquad (8)$$

For compacting aquifer systems, $S'_{skv} >> S_{sw}$ (specific storage of water), and the inelastic storage coefficient of the aquifer system is approximately equal to the inelastic aquitard skeletal storage coefficient, $S_v \cong S'_{kv}$. In confined aquifer systems subject to large-scale overdraft, the volume of water derived from permanent aquitard compaction can typically range from 10 to 30 percent of the total volume of water pumped and represents a one-time mining of stored ground water and a small permanent reduction in the storage capacity of the aquifer system.

In unconfined aquifer systems the skeletal storage coefficients described above also govern the compressibility of the fine-grained sediments below the water table and contribute to the volume of water released from storage when heads decline, and is defined by the specific yield, Sy, of the aquifer system. Water derived from storage in unconfined aquifer systems primarily results from the gravity drainage of pore water from the sediments and its value is typically in the range of 0.1–0.3, somewhat less than the porosity, and somewhat greater than the specific retention of the sediments. Typically, $S_y >> S$ by two to three orders of magnitude.

For confined and unconfined aquifers, the IBS1 Package requires that storage coefficient terms be specified for the elastic skeletal storage coefficient (S_{ke}), and inelastic aquitard skeletal storage coeffficient (S'_{kv}) (Leake and Prudic, 1991). For confined aquifers, in order to account for the component of storage related to the compressibility of water, S_w was entered as the storage coefficient in the BCF package of MODFLOW. Within MODFLOW these three storage components (S_{ke}, S'_{kv}, and S_w) are summed and the storage coefficient of the aquifer system, S, is implemented for each model layer. For unconfined aquifers, IBS1 requires the two components of the skeletal storage coefficient. In contrast with the procedure used to implement the aquifer-system storage coefficient for confined aquifers, the specific yield (S_y) was entered as the storage term in the input file for the BCF package for layer 1, and this value was used by the model where and when unconfined aquifer conditions occurred in that model layer. Note that the specific yield of an unconfined aquifer is many orders of magnitude greater than storage coefficient associated with the compressibility of water. Therefore, the water released from storage owing to the expansion of water is negligible with respect to the amount released by the gravity drainage of pore water. In this model, it was assumed that compaction occurs only in layers 1 and 2. Because little pumping occurs in layer 3 and because sediments in layer 3 have been subjected to fairly large overburden stress, it was assumed that there is little potential for compaction of this layer.

The initial storage coefficients for the model were calculated using specific-storage values obtained from one-dimensional (Sneed and Galloway, 2000) and three-dimensional (Nishikawa and others, 2001) models of ground-water flow and aquifer-system compaction at Edwards Air Force Base. The specific storage values range from 4.2×10^{-7} ft^{-1} for the compressibility of water (S_{sw})to 3.5×10^{-4} ft^{-1} for the inelastic skeletal specific storage (S'_{skv}) of thick (greater than 18 ft) aquitards (table 4). The initial storage coefficients for the compressibility of water (S_w) and elastic skeletal storage (S_k) for layers 1 and 2 were calculated as the product of the respective specific-storage value and the saturated thickness of the layer. The initial inelastic aquitard skeletal storage coefficients (S'_{kv}) were calculated as the product of the inelastic specific storage of thick aquitards and the estimated total thickness of aquitards within the aquifer.

Table 4. Specific storage values used in calculating storage coefficients for layers 1 and 2 in the ground-water flow model of the Antelope Valley ground-water basin, California

[Data from Sneed and Calloway, 2000; Nishikawa and others, 2001. ft^{-1}, per foot]

	Specific storage (ft^{-1})
Compressibility of water...........	4.2×10^{-7}
Elastic skeletal specific storage..	1.7×10^{-6}
Inelastic skeletal specific storage for thin aquitards (less than or equal to 18 feet thick)	4.0×10^{-5}
Inelastic skeletal specific storage for thick aquitards (greater than 18 feet thick)	3.5×10^{-4}

The total thickness of the aquitards in layers 1 and 2 was estimated from the percentage of the fine-grained sediments in these layers that was determined from descriptions of the aquifer material noted in selected well drillers' logs. The percentage of fine-grained sediments ranged from 13 to 50 percent of the thickness of each layer. The inelastic aquitard skeletal storage coefficient was specified only for those areas of layers 1 and 2 where subsidence of more than 1 ft had been measured in the study area (fig. 8). Compaction was not simulated for layer 3; therefore, the storage coefficient for layer 3 was estimated by multiplying the specific storage of the aquifer by the thickness of the layer (550 ft). A specific storage of 2.0×10^{-6} ft^{-1} was assumed representative of the aquifer materials in layer 3, resulting in a storage coefficient of 1.0×10^{-3}. This value was used throughout layer 3, regardless of the thickness of the layer, except for the model area near Rogers Lake, north of the Willow Springs Fault. The storage coefficient calibrated by Nishikawa and others (2001) during the simulation of ground-water flow and land subsidence at Edwards Air Force Base (5.71×10^{-4}) was used in the model area north of Willow Springs Fault.

Specific-yield values used in the Durbin (1978) model for the unconfined aquifer ranged from 0.05 to 0.20: these values were used as initial values for the upper aquifer. Microgravity measurements collected from 1996–98 as part of an injection, storage, and recovery test at Lancaster were used to estimate a specific yield of about 0.13 (Howle and others, 2003).

Preconsolidation Head

As noted earlier, inelastic compaction of compressible sediments occurs when water levels decline below the preconsolidation head. Accurate estimates of preconsolidation head values are critical for the simulation of subsidence (Sneed and Galloway, 2000); the initial values of preconsolidation head for the model were based on results from the one-dimensional model of ground-water flow at Edwards Air Force Base (Sneed and Galloway, 2000). Initial preconsolidation head values were specified from 0 to 50 ft below pre-development water levels only for those areas that have 1 ft of measurable subsidence (fig. 8). If future water levels decline below preconsolidation heads outside the areas of subsidence shown in figure 8, then subsidence may occur in those areas. The magnitude and distribution of preconsolidation heads for the areas that have no measurable subsidence are not known and, therefore, calibration of preconsolidation heads for these areas is not possible. Subsidence was not simulated for those areas because there is no constraint for the range of preconsolidation heads.

Horizontal-Flow Barriers

Nine faults that transect the ground-water basin were simulated as partial barriers to ground-water flow (fig. 11, table 5). The Horizontal-Flow Barrier (HFB) package (Hsieh and Freckleton, 1993) was used to simulate these faults as horizontal-flow barriers. The HFB package allows for the simulation of thin, vertical, low-permeability geologic features, such as vertical faults and fine-grained material, that act as partial barriers to horizontal ground-water flow. The function of each simulated barrier is to lower the horizontal conductances between two adjacent model cells. The barriers are defined by a hydraulic characteristic, which for unconfined aquifers is the hydraulic conductivity of the fault divided by the width of the fault and for confined aquifers is the transmissivity of the fault divided by the width of the fault. Each barrier may be subdivided into segments and each segment may have a different hydraulic characteristic. All the barriers simulated in the model were assumed to extend through all three model layers. The hydraulic characteristic value for each segment (table 5) was determined by model calibration.

The simulated barriers include an unnamed fault between Finger Buttes and West Antelope subbasins (barrier 1), the Randsburg–Mojave Fault (barrier 2), the Neenach Fault (barrier 3), and an unnamed fault between the Buttes and Pearland subbasins (barrier 4) (fig. 11, table 5). These four barriers were simulated as partial barriers to ground-water flow in the Durbin (1978) model. The fault separating the Buttes and Pearland subbasins from the Lancaster subbasin (fig. 11) was not simulated as a barrier to flow in the Durbin (1978) model. This fault also was not simulated as a barrier to flow in this model. Five of the faults simulated as partial barriers to flow were not simulated as barriers in the Durbin (1978) model. These faults include the extensions of the Muroc Fault (barrier 5) and the El Mirage Fault (barrier 6) across Rogers Lake and an extension of the Willow Springs fault from the northwest corner of Rosamond Lake southeast along the southern edge of Buckhorn Lake to the eastern edge of the study area (barrier 7). These faults were simulated as partial barriers to flow in the Edwards Air Force Base model (Nishikawa and others, 2001). Two additional partial barriers to flow were inferred from water-level data and model calibration; one barrier southeast of Lovejoy Buttes, parallel to the northeast boundary of the Buttes subbasin (barrier 8), and one barrier south of Rosamond Lake, trending northwest-southeast from the Neenach Fault to the eastern edge of the study area (barrier 9). These barriers are believed to be related to faults that are not exposed at land surface.

Model Stresses

Hydraulic heads in the ground-water flow system respond to stresses on the system, which correspond to recharge and discharge. As noted earlier, recharge to the ground-water system includes natural recharge from mountain-front runoff and stream infiltration in the upper reaches of ephemeral streams and artificial recharge of irrigation-return flow and treated wastewater. Discharge from the ground-water systems includes evapotranspiration, ground-water outflow, and ground-water pumpage.

Natural Recharge

Natural recharge from mountain-front runoff and stream infiltration was simulated as areal recharge to layer 1, the location of the recharge cells are shown in figure 12. The initial value of total annual natural recharge was assumed to be 40,700 acre-ft, the value simulated in the Durbin (1978) model. The distribution of natural recharge was based on the location and size of the intermittent streams used to estimate natural recharge (Durbin, 1978). The initial annual recharge specified for these cells ranged from 65 to 3,800 acre-ft for each cell. Natural recharge did not vary from year to year because data were limited, which precluded simulating seasonal or annual variations in natural recharge. Results from a study by Bouwer (1982) indicate that seasonal and annual fluctuations in infiltration are attenuated as a function of sediment particle size in the unsaturated zone and vertical distance to the water table. Natural recharge was not specified for the entire reach of streams in the basin because the streams are intermittent and flow does not always occur over the entire length of the stream.

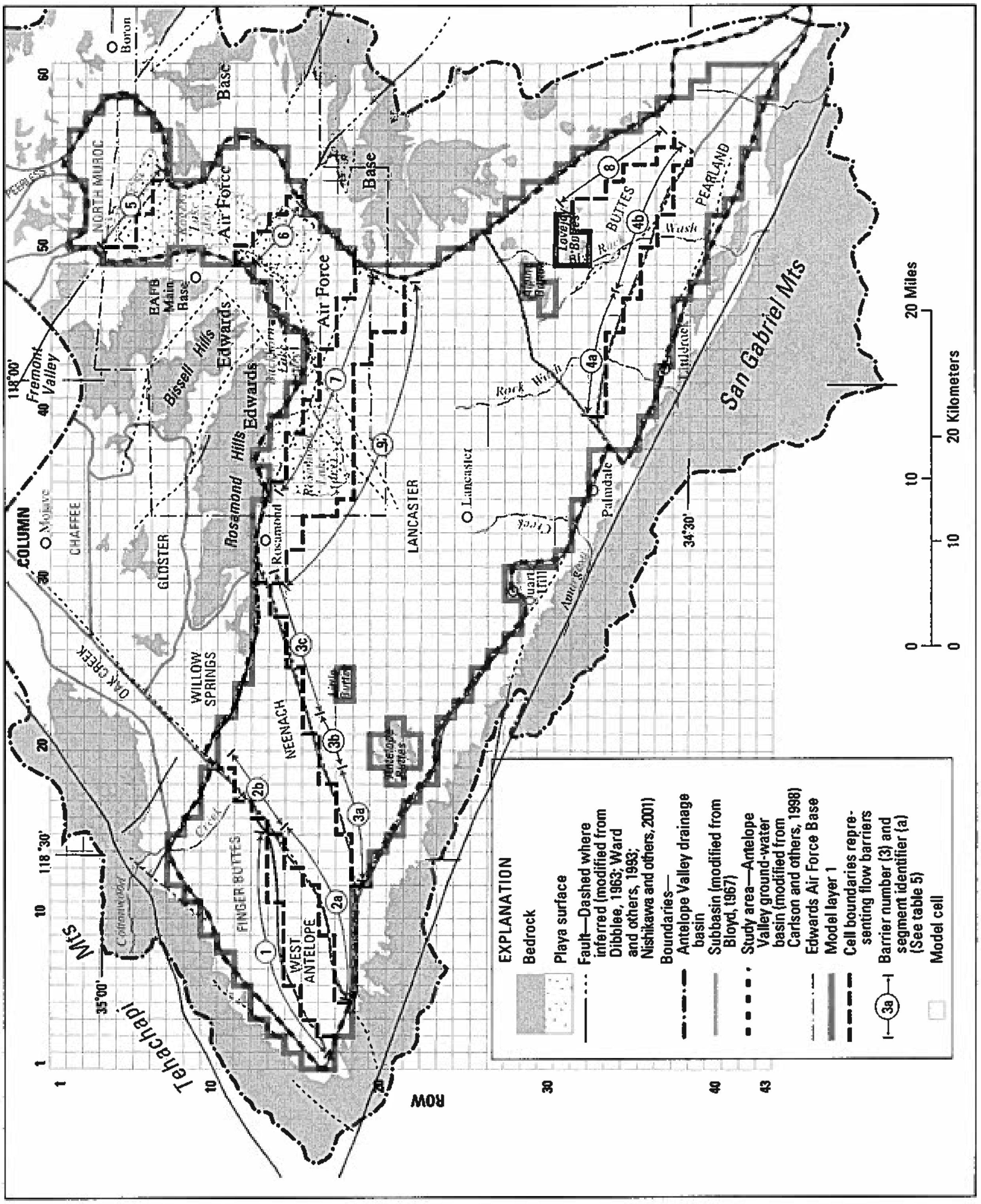

Figure 11. Location of barriers to horizontal ground-water flow simulated in the ground-water flow model of the Antelope Valley ground-water basin, California.

Table 5. Hydraulic characteristics of the horizontal-flow barriers simulated in the ground-water flow model of the Antelope Valley ground-water basin, California

[d^{-1}, per day; ft/d, foot per day. —, no barrier simulated in this layer]

Barrier No.	Segment	Barrier name	Hydraulic characteristic		
			Layer 1 (d^{-1})	Layer 2 (ft/d)	Layer 3 (ft/d)
1		([1])	0.00008	0.0008	0.0008
2	a	Randsburgq–Mojave Fault	.00007	.0007	.0007
	b		.00002	.0002	.0002
3	a	Neenach Fault	.0008	.008	.008
	b		.002	.02	.02
	c		.004	.04	.04
4	a	([1])	.0004	—	—
	b		.0003	—	—
5		Muroc Fault	.001	.01	.01
6		El Mirage Fault	.001	.01	.01
7		Willow Springs Fault	.0001	.001	.001
8		([1])	.00001	—	—
9		([1])	.00001	.0001	—

[1] Unnamed

Artificial Recharge

Artificial recharge in the ground-water basin, as noted earlier, includes the infiltration of irrigation-return flows of pumped ground water and imported water used for agriculture and treated wastewater discharged to spreading ponds.

Irrigation-Return Flow

Irrigation-return flow is that portion of the water applied to crops that is not consumptively used by the crops. Irrigation efficiency, which is defined as the percentage of applied water used by the crops, was assumed to be 70 percent, leaving as much as 30 percent of the applied irrigation water available to return to the water table as irrigation-return flow. In Antelope Valley, most of the applied water is for the production of alfalfa. The irrigation efficiency was estimated on the basis of the quantity of irrigation water applied to alfalfa [approximately 6.6 ft/yr (Orloff and others, 1989)] and the quantity of water consumed by alfalfa [approximately 4.8 ft/yr (table 2)]. Estimates of irrigation efficiency by Snyder (1955) and by the California Department of Public Works (1955) were about 50 percent; however, consumptive-use estimates at the time of these two studies (3.4–3.6 ft/yr) were lower than current estimates (4.8 ft/yr). The current consumptive-use estimates were considered more accurate than the consumptive-use estimates used by researchers in the 1950s; therefore, an irrigation efficiency of 70 percent was assumed valid for the entire simulation period.

Because pumpage has caused ground-water levels to decline more than 100 ft throughout most of the ground-water basin and owing to the existence of thin aquitards within the aquifers, recharge from water applied for agriculture probably did not reach (recharge) the water table until about 10 years after application. The actual delay in irrigation-return flow reaching the water table probably is variable depending on the depth to water and the existence of fine-grained layers in the unsaturated zone. Irrigation-return flows were simulated as wells that had positive flow rates (i.e., flow recharging the ground-water flow system) at the cells where agricultural pumpage was simulated (fig. 5). The areas that had irrigation-return flows remained constant during 1915–51 but varied annually during 1952–95. Annual agricultural recharge varied from 0 to 111,000 acre-ft.

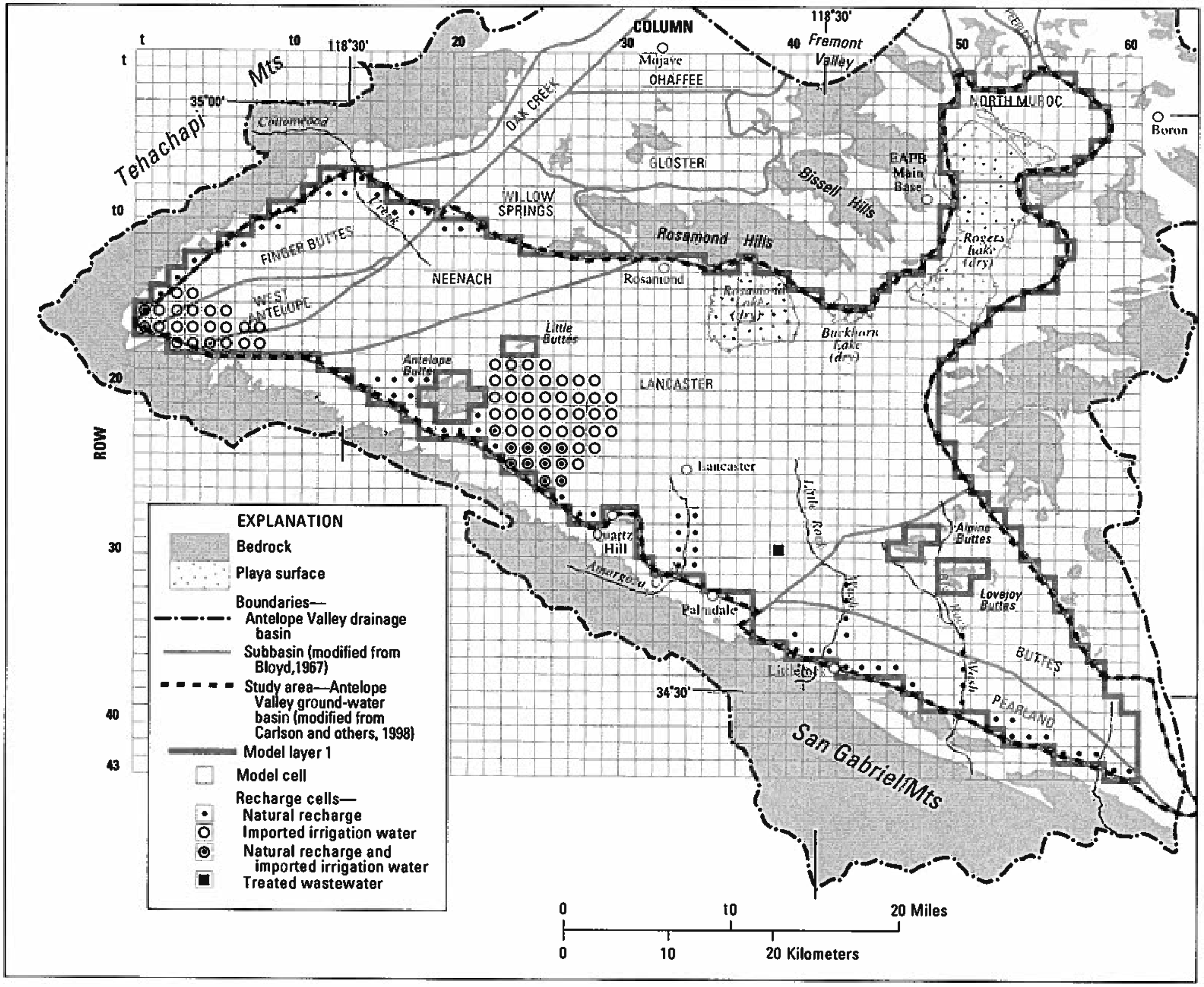

Figure 12. Location of model cells used to simulate natural recharge, recharge of imported water used for irrigation, and recharge of treated wastewater in the ground-water flow model of the Antelope Valley ground-water basin, California.

Beginning in 1972, water was imported from northern California to Antelope Valley by way of the California aqueduct. Records of deliveries of imported water from the Antelope Valley–East Kern Water Agency (AVEK) show that growers began using large quantities of imported surface water in 1976. The records also indicate that most of the imported water was delivered to two areas of the valley; (1) the western part of the Lancaster subbasin, east of Antelope Buttes, and (2) the far western part of the study area, in the Finger Buttes, Neenach, and West Antelope subbasins (fig. 12). Thirty percent of the annual imported water delivered to these areas was specified as irrigation-return flow and was simulated as wells that had positive flow rates into layer 1 of the model 10 years after the water was applied at land surface.

Treated Wastewater

The estimated annual quantity of treated wastewater that could infiltrate into the unsaturated zone is shown in table 1. The treated wastewater is from urbanized parts of the study area that are served by the water reclamation plants. Recharge from septic systems in the rural parts of the study area was assumed to be negligible. Recharge from treated wastewater was assumed to reach the water table in the year that it was applied at land surface because this source of water is essentially constant and the rate of infiltration per acre is much greater than that for agriculture. Recharge from the Palmdale Water Reclamation Plant was applied to only one cell (fig. 12) for 1984–95, the years in which recharge from the treated wastewater was estimated to occur (table 1). On the basis of results of infiltration studies at the Lancaster Water Reclamation Plant, the assumption was made that recharge of treated wastewater from the plant does not reach the regional water table, and, therefore, it was not simulated for this site.

Natural Discharge

Evaporation from bare-soil and transpiration by phreatophytes in areas were the water table was near land surface were simulated using the Evapotranspiration Package developed by McDonald and Harbaugh (1988). These areas were identified using maps that show the area of flowing wells in 1908 (Johnson, 1911) and alkali soils (Durbin, 1978) (fig. 13). Estimates of evapotranspiration rates in Antelope Valley were based on results reported by Lines and Bilhorn (1996) in the nearby Mojave River Basin. An annual maximum evapotranspiration rate of 0.6 ft/yr was specified when the water table was at land surface and was decreased linearly to zero when the water table reached a depth of 10 ft below land surface.

Durbin (1978) estimated that 1,000 acre-ft/yr of ground water is discharged as ground-water underflow north of Rogers Lake into Fremont Valley: this estimate was based on the water-level gradient and the cross-sectional area of the aquifer. Water-level data from nearby wells indicate that the gradient at that location has not been constant over time, which suggests that subsurface ground-water flow has not been constant (Nishikawa and others, 2001). Variable subsurface ground-water flow was specified in the transient-state simulation using a time-varying specified-head cell (fig. 13). The water level at the specified-head cell (fig. 14) was based on water-level data from nearby wells (Nishikawa and others, 2001), and flow out of the study area into Fremont Valley was calculated by the model using the gradient between the specified-head cell and adjacent active cells.

Pumpage

Total annual pumpage specified in the model is shown in figure 5. The spatial distribution of pumpage for 1915–51 was based on the Durbin (1978) model. The spatial distribution of pumpage for 1915–51 was concentrated primarily in agricultural areas and did not vary over time. The spatial distribution of pumpage for 1952–95 was based on the spatial distribution of pumpage in the database created by Templin and others (1995) and updated for this study (see Appendix: Water Use 1992–95). The pumpage database contains annual pumpage data for individual wells and information on the location of these wells. Well location data allowed the spatial distribution of pumpage in the model to vary for 1952–95, years when the primary pumping centers moved from agricultural areas to urban areas. The pumpage database, however, does not contain data for all agricultural pumpage in the study area; therefore, land-use data were used in conjunction with the database to simulate the distribution of agricultural pumpage.

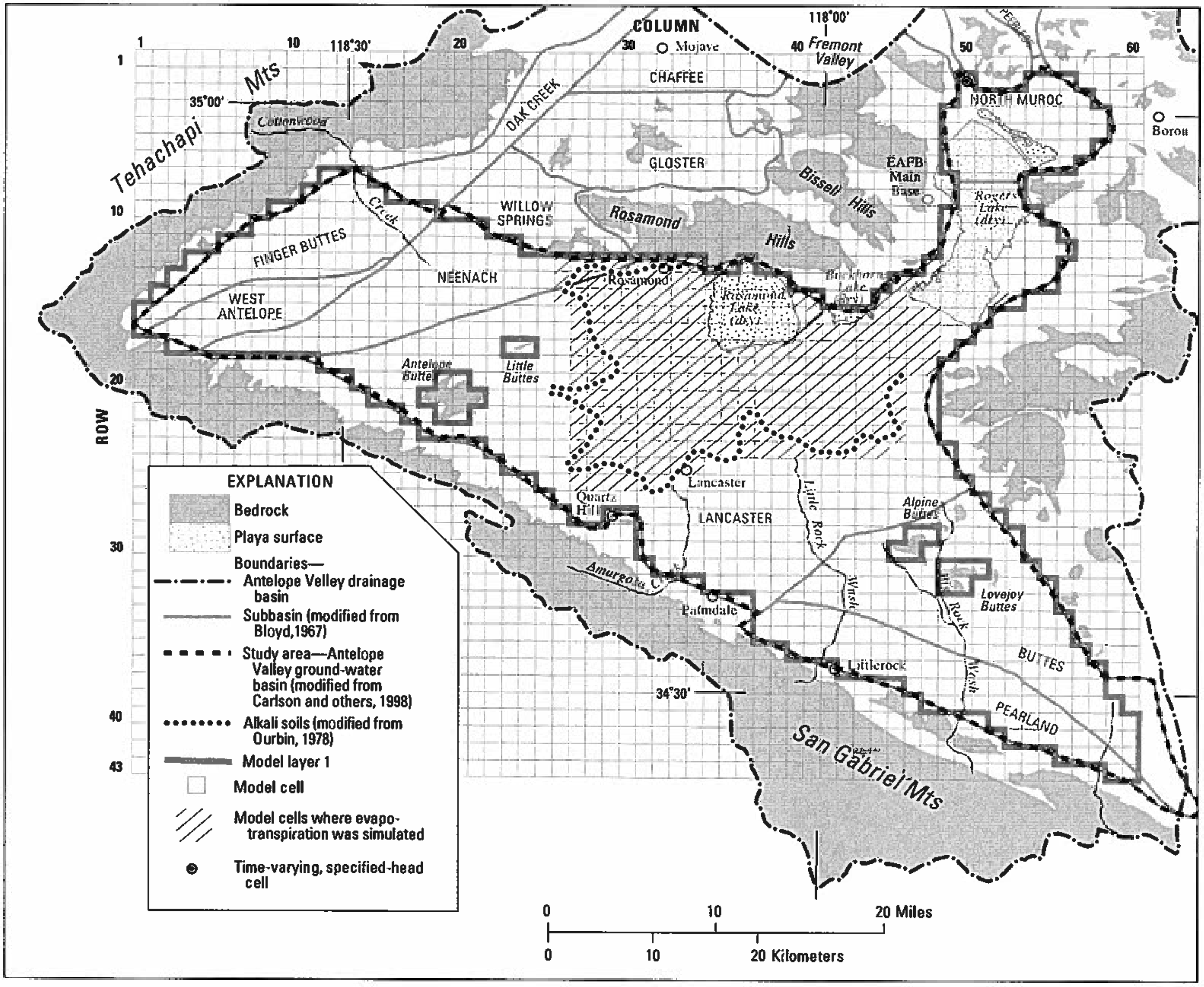

Figure 13. Location of model cells used to simulate natural ground-water discharge in the ground-water flow model of the Antelope Valley ground-water basin, California.

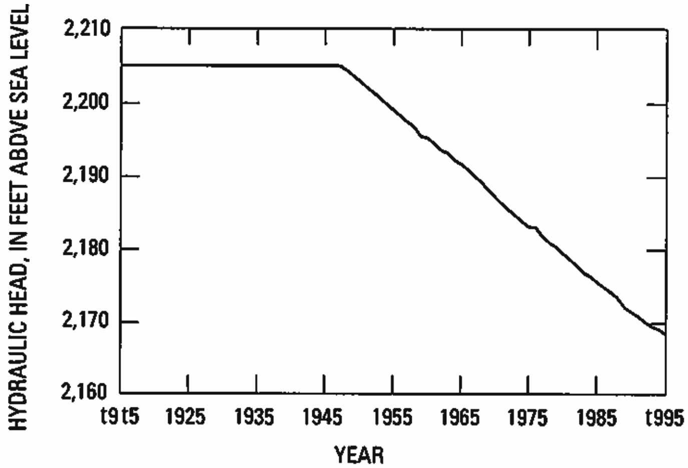

Figure 14. Time-varying specified hydraulic head used for the north boundary of the ground-water flow model of the Antelope Valley ground-water basin, California (modified from Nishikawa and others, 2001).

A comparison of the spatial distribution of pumpage in the database and land-use data for 1961 and 1987 indicated that the database does not have pumpage data for areas of agricultural land use in the West Antelope and the western Neenach subbasins. The land-use data showed that about 6.8 percent of the total agricultural land in the study area was in these areas; therefore, the annual agricultural pumpage for these areas was assumed to be 6.8 percent of the total annual agricultural pumpage. Agricultural pumpage in the West Antelope and the western Neenach subbasins was distributed to model cells corresponding to the location of the agricultural land use. Pumpage in these areas was assumed to have occurred between 1934 and 1986: this assumption was based on a comparison of simulated water levels and measured water levels for well 8N/17W-1N1 (well location shown in fig. 15) in the West Antelope subbasin.

The spatial distribution and quantity of pumpage for public supply for 1919–91was determined from the pumpage database compiled by Templin and others (1995) and for 1992–95 from water-use information compiled for this study (Table A1 in the Appendix). The location and quantity of pumpage from public supply wells is well documented, and was not changed during the calibration process.

Because there was limited well-construction data available, all wells were assumed to be fully perforated in both layers 1 and 2. The proportion of pumpage from a layer was determined by dividing the transmissivity of that layer by the sum of the transmissivity of layers 1 and 2. The transmissivity of layer 1 was calculated as the product of hydraulic conductivity and initial (1915) saturated thickness. The vertical distribution of pumpage from layers 1 and 2 varied spatially but did not vary with time; therefore, a limitation of this approach is that the vertical distribution of pumpage does not change as the water table declines. In the aquifer system, changes in the saturated thickness of the upper aquifer changes the transmissivity of the upper aquifer, which affects the flow of water to wells. It was assumed that there was no pumpage from layer 3 because few wells in Antelope Valley are deep enough to penetrate the lower aquifer and because the transmissivity of this layer is low. This assumption is valid particularly for the earlier part of the simulation period when rates for total annual pumpage were highest. During the latter part of the simulation period, wells were drilled in the lower aquifer (layer 3) and thus some pumping occurred from this aquifer. The limited pumping that occurred only from the lower aquifer was simulated as pumpage from layers 1 and 2.

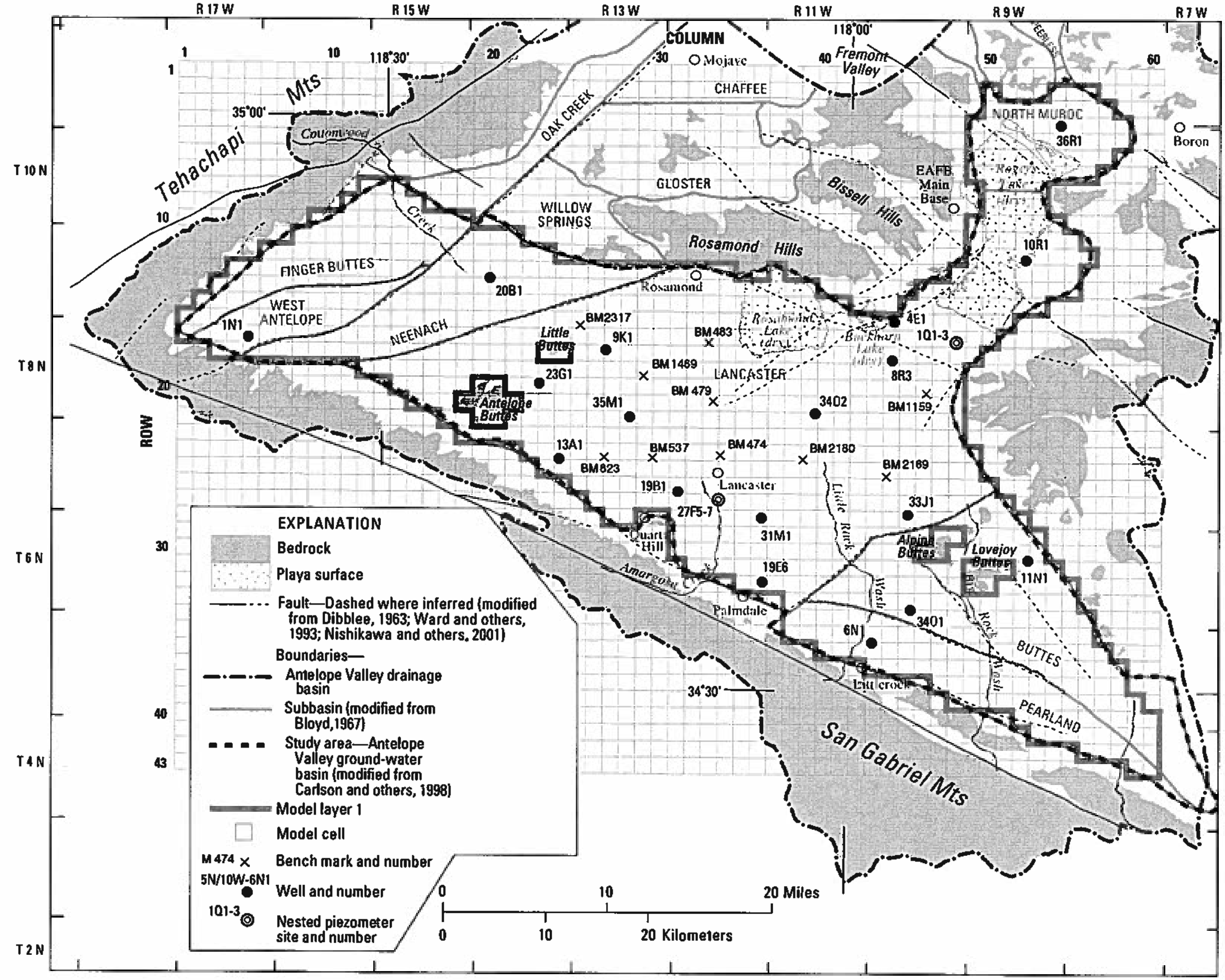

Figure 15. Location of wells and bench marks used to calibrate the transient-state model of the Antelope Valley ground-water basin, California.

Model Calibration

Model calibration is the process of making adjustments, within justifiable ranges, to initial estimates of selected model parameters and stresses to obtain reasonable agreement between simulated and measured values (for this model, water levels and land subsidence). Modifications were made to the initial estimates of the hydraulic conductivity of layer 1, the transmissivity of layer 2, specific yield, natural recharge, aquitard thickness, hydraulic characteristics of horizontal flow barriers, and preconsolidation head using a trial-and-error approach. Vertical leakance was recalculated after changes were made to any of the values used to calculate vertical leakance; hydraulic conductivity, transmissivity, or saturated thickness. The values of transmissivity and storage coefficient of layer 3 were not changed from the initial values during the model calibration process because reasonable changes in these values had negligible affect on model results.

Prior to 1915, there was little ground-water development in Antelope Valley and the ground-water flow system was in a time-averaged state of equilibrium. Inflows from recharge were balanced by outflows as evapotranspiration and ground-water underflow, and water levels were essentially unchanging. This state of equilibrium was simulated by the steady-state model that represents conditions in 1915. The addition of stress to the ground-water flow system owing to pumping resulted in an imbalance between inflows and outflows, which disturbed the state of equilibrium and resulted in time-varying or transient-state conditions. Ground-water conditions during the period 1915–95 were simulated with a transient-state model. During the calibration process both steady-state and transient-state simulations were used: the steady-state simulation was used to provide initial conditions for the transient-state simulation. Any changes made to the transient-state simulation were incorporated into the steady-state simulation and the steady-state simulation was rerun to ensure that the changes made during the transient-state simulation produced reasonable results for steady-state conditions. This process was repeated until a satisfactory match between measured and simulated results was obtained.

Steady-State Simulation

The steady-state simulation of 1915 conditions was made to provide initial conditions for the transient-state simulation. The steady-state simulation requires initial estimates of hydraulic conductivity, transmissivity, vertical leakance, hydraulic characteristics of horizontal flow barriers, natural recharge, and evapotranspiration (maximum evapotranspiration rate and extinction depth). Storage coefficients are not required for a steady-state simulation.

For this study, only estimates of natural recharge and evapotranspiration were modified during the initial steady-state calibration. Initial estimates of hydraulic conductivity, transmissivity, vertical leakance, and hydraulic characteristics were modified during the transient-state calibration. A subsequent steady-state simulation was then run to verify that the changes made during the transient-state simulation to these parameters resulted in a reasonable steady-state simulation of 1915 conditions. Ground-water level measurements, made around 1915, from 21 wells were used to determine if the steady-state simulation provided reasonable initial conditions for the transient-state simulation (fig. 16, table 6).

The final calibrated distribution of natural recharge is shown in figure 17; recharge ranged from 65 to 3,250 acre-ft/yr per cell.Total natural recharge in the calibrated steady-state simulation was 30,300 acre-ft/yr, 10,400 acre-ft/yr less than the natural recharge simulated in the Durbin (1978) model (40,700 acre-ft/yr). Most of the reduction in simulated natural recharge occurred in the Pearland and Buttes subbasins; natural recharge was decreased from an initial estimate of 26,500 acre-ft/yr (Durbin, 1978) to 16,200 acre-ft/yr. Simulated water levels were higher than the measured water levels in these subbasins when the initial value of natural recharge was simulated. No reasonable combination of hydraulic conductivity, transmissivity, and values of hydraulic characteristic of flow barriers resulted in acceptable simulated water levels for these subbasins when the initial value of natural recharge was used in the steady-state simulation.

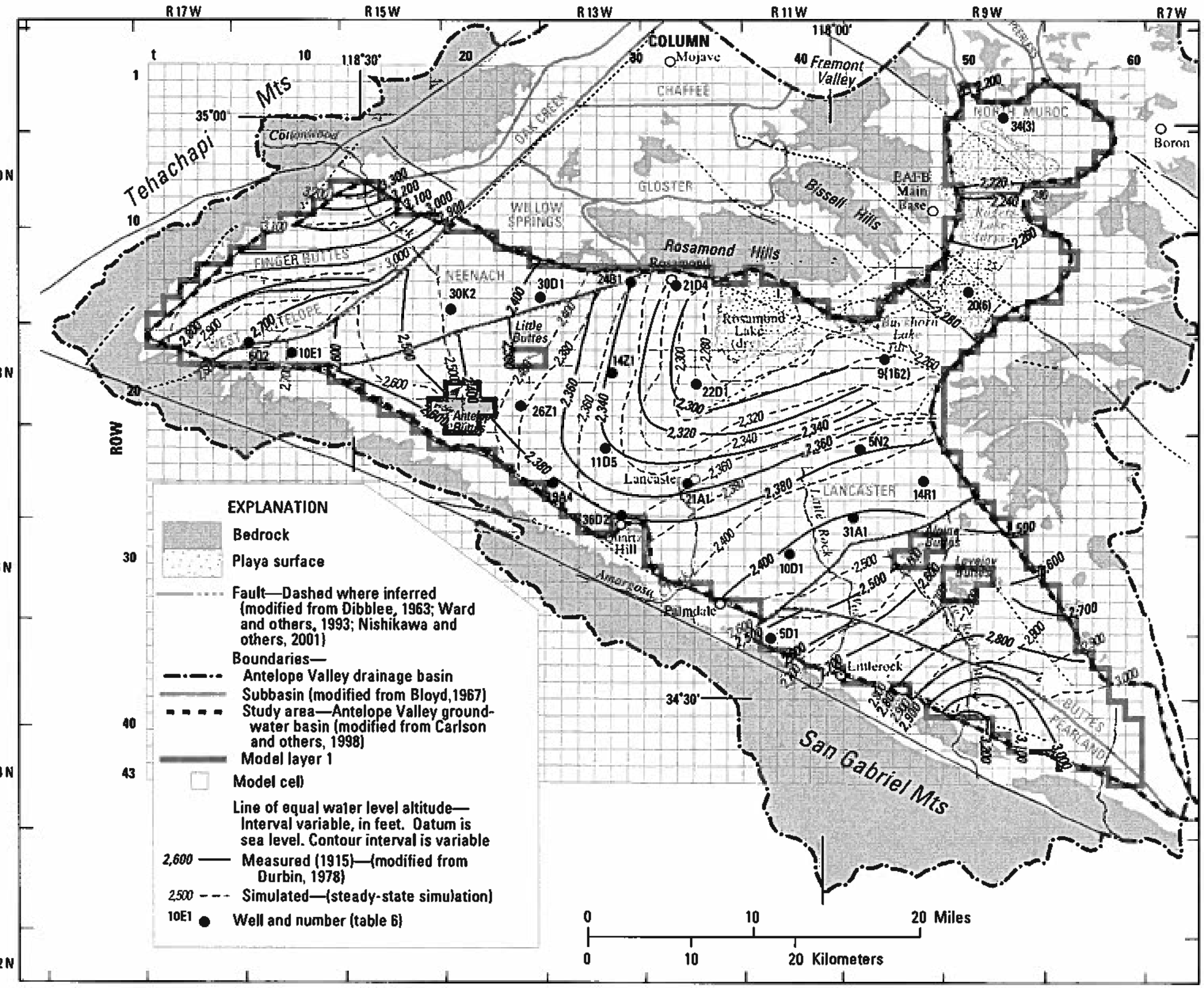

Figure 16. Location of wells used to calibrate the steady-state simulation and measured and simulated steady-state water levels from the ground-water flow model of the Antelope Valley ground-water basin, California.

Table 6. Measured and simulated (layer 1) water levels for wells used to calibrate the steady-state simulation of the ground-water flow model of the Antelope Valley ground-water basin, California

[State well No.: see well-numbering diagram; see figure 17 for location of wells; well depth in feet below land surface; water levels in feet above sea level; —, no data]

State well No.	Subbasin	Well depth	Year of measurement	Water levels		Difference, feet
				Measured	Simulated	
5N/11W-5D1	Pearland	403	1917	2,600	2,630	30
6N/11W-10D1	Lancaster	445	1915	2,430	2,434	4
7N/10W-5N2	Lancaster	404	1921	2,380	2,381	1
7N/10W-14R1	Lancaster	—	1921	2,403	2,414	11
7N/10W-31A1	Lancaster	300	1921	2,421	2,424	3
7N/12W-21A1	Lancaster	301	1915	2,354	2,346	−8
7N/13W-11D5	Lancaster	351	1917	2,341	2,351	10
7N/13W-19A4	Lancaster	75	1908	2,368	2,367	−1
7N/13W-36D2	Lancaster	466	1914	2,368	2,356	−12
8N/10W-9 (162)[1]	Lancaster	25±	1921	2,303	2,308	5
8N/12W-22D1	Lancaster	371	1910	2,278	2,283	5
8N/13W-14Z1	Lancaster	200	1907	2,348	2,357	9
8N/14W-26Z1	Lancaster	—	1909	2,376	2,382	6
8N/16W-6Q2	West Antelope	302	1909	2,824	2,847	23
8N/16W-10E1	Neenach	—	1909	2,682	2,701	19
9N/9W-20 (6)[1]	Lancaster	—	1917	2,275[3]	2,253	−22
9N/12W-21D4	Lancaster	89	1909	2,316	2,318	2
9N/13W-24B1	Lancaster	63	1908	2,359	2,353	−6
9N/13W-30D1	Neenach	62	1908	2,400	2,439	39
9N/14W-30K2	Neenach	255	1908	2,445	2,494	49
11N/9W-34 (3)[1]	North Muroc	260	—[2]	2,196	2,224	28

[1]Number in parenthesis is the map number of the well as recorded by Thompson (1929, p. 348)
[2]Measured after 1915; Thompson (1929, p. 364)
[3]Flowing

The initial maximum simulated evapotranspiration rate of 0.6 ft/yr and extinction depth of 10 ft below land surface were unchanged. Specifying a higher maximum rate had little effect on model results, and specifying a lower maximum evapotranspiration rate resulted in simulated water levels that were significantly higher than the measured water levels.

The simulated steady-state water levels for layer 1 ranged from 22 ft lower to 49 ft higher than the measured water levels (table 6). The simulated water levels for wells in the Lancaster subbasin were within 12 ft of the measured water levels except for well 9N/9W-20(6) for which the simulated water levels were 22 ft lower than the measured water levels. The simulated water levels ranged from 19 to 49 ft higher than the measured water levels in wells in the Neenach and West Antelope subbasins. The simulated water level for the single calibration well in the Pearland subbasin was 30 ft higher than the measured water level. The differences between the simulated and measured water levels in the Neenach, West Antelope, and Pearland subbasins were large because hydrologic data for these subbasins were limited. For wells in the Buttes and Finger Buttes subbasins, there were no water-level measurements available to calibrate the steady-state model.

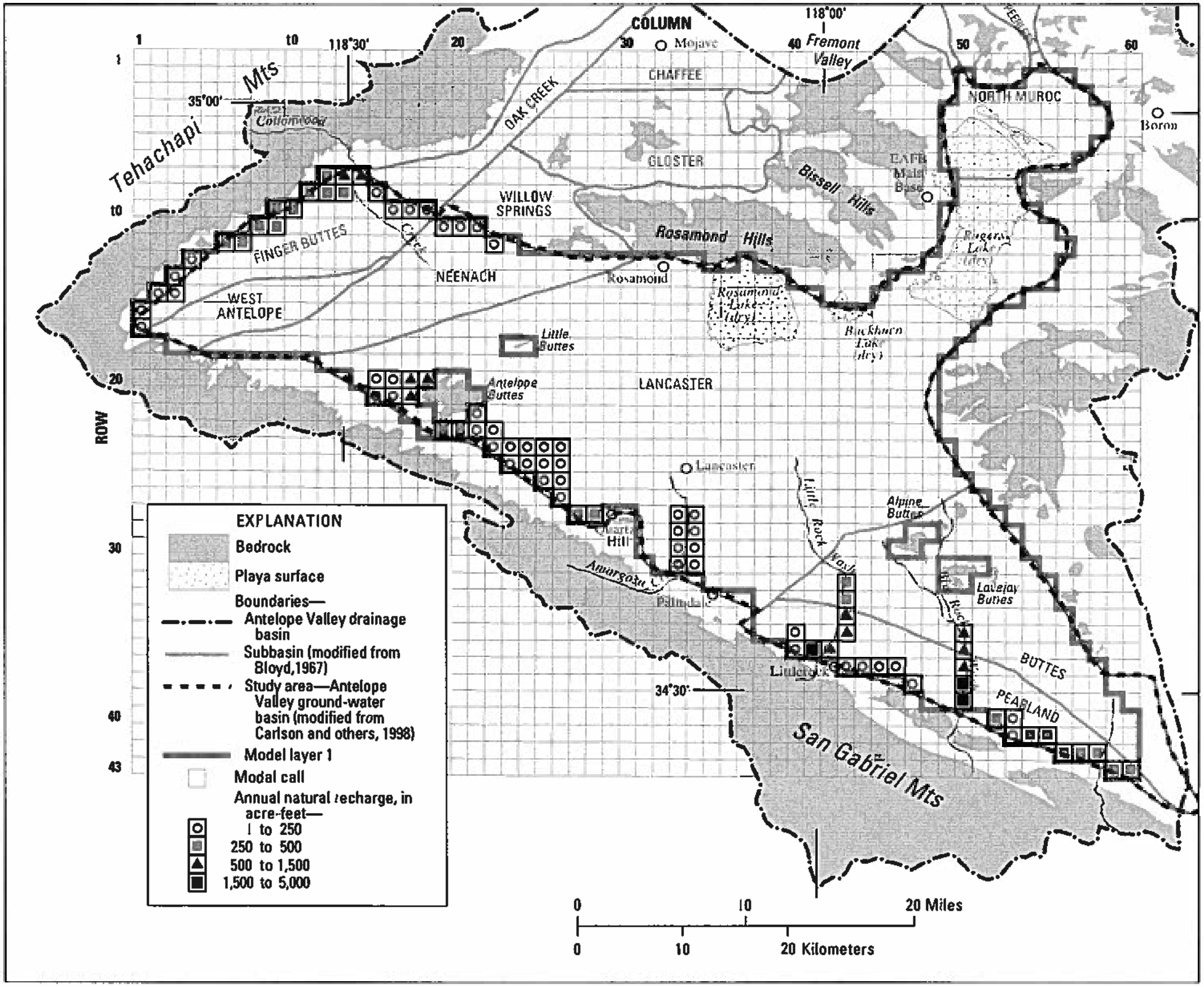

Figure 17. Areal distribution of natural recharge specified in the ground-water flow model of the Antelope Valley ground-water basin, California.

Contours of measured and simulated layer 1 water levels for 1915 are plotted together for comparison purposes on figure 16. Ground-water flow direction inferred from the contours of simulated water levels is similar to flow direction inferred from the 1915 measured water-level contours. Ground-water flow is from recharge areas along the valley margins to discharge areas around the playas and the north boundary of the model. In the north Lancaster and North Muroc subbasins, the simulated water-level gradient to the north is less than the measured gradient. The largest differences between the measured and simulated water-level contours are in the Finger Buttes and Pearland subbasins: in these subbasins, the simulated water-level gradient is less than the measured gradient. The accuracy of the measured 1915 water-level contours for these two subbasins, however, is uncertain owing to the lack of available water-level data.

Transient-State Simulation

Calibration of the transient-state model involved trial-and-error adjustments of horizontal hydraulic conductivity, transmissivity, vertical leakance, storage coefficient, hydraulic characteristic of barriers, preconsolidation head, and artificial recharge of irrigation-return flows. New values of vertical leakance were calculated during the calibration process to incorporate changes in the hydraulic conductivity and saturated thickness of layer 1 and the transmissivity of layers 2 and 3. Model parameters for the area north of Willow Springs Fault (barrier 7 on figure 11) were modified from values used in the Edwards Air Force Base ground-water flow and land subsidence model (Nishikawa and others, 2001).

The transient-state model was calibrated using available water-level data from 24 wells for the period 1915–95 and subsidence data from 10 bench marks for the period 1926–92 (fig. 15). Data from 19 of the 24 wells were used to compare measured and simulated water levels over time; the wells were selected on the basis of the length of water-level records and the spatial distribution of the wells. Data from two nested piezometer sites (wells 7N/12W-27F5–27F7 near Lancaster and wells 8N/10W-1Q1–1Q3 south of Rogers Lake) were used to compare the simulated and measured vertical hydraulic-head gradient between layers. The selection of the bench marks was based on the length of subsidence record and spatial distribution of the bench marks. The transient-state model was assumed to be calibrated when the simulated water levels matched the general magnitude and trend of the measured water levels, the general flow directions inferred from contours of the simulated water levels matched flow directions inferred from the contours of measured water levels, the onset and magnitude of land subsidence matched measured land subsidence, and the model parameters were within reasonable limits supported by the available geohydrologic data.

The calibrated values of the horizontal hydraulic conductivities used for layer 1 ranged from 2 to 30 ft/d (fig. 18). Modifications were made to the initial values of horizontal hydraulic conductivity primarily for the areas southwest, south, and east of Rosamond Lake and for the Buttes subbasin. For these areas, few, if any, aquifer-test data were available to estimate the transmissive properties of the aquifer. In the area around Rosamond Lake, water levels that were simulated using the initial values of horizontal hydraulic conductivity were too low; therefore, the initial values were decreased to increase the simulated water levels. Lacustrine deposits are present in the upper aquifer in this part of the basin (fig. 3), which may explain the low simulated hydraulic conductivity values. In the southeast part of Buttes subbasin, the horizontal hydraulic conductivity was decreased from an initial value of 10 ft/d to a value of 2 ft/d. In the northwest part of the subbasin, horizontal hydraulic conductivity was increased from an initial value of 25 to 30 ft/d in order to lower simulated water levels in the northwestern parts of the Buttes and Pearland subbasins.

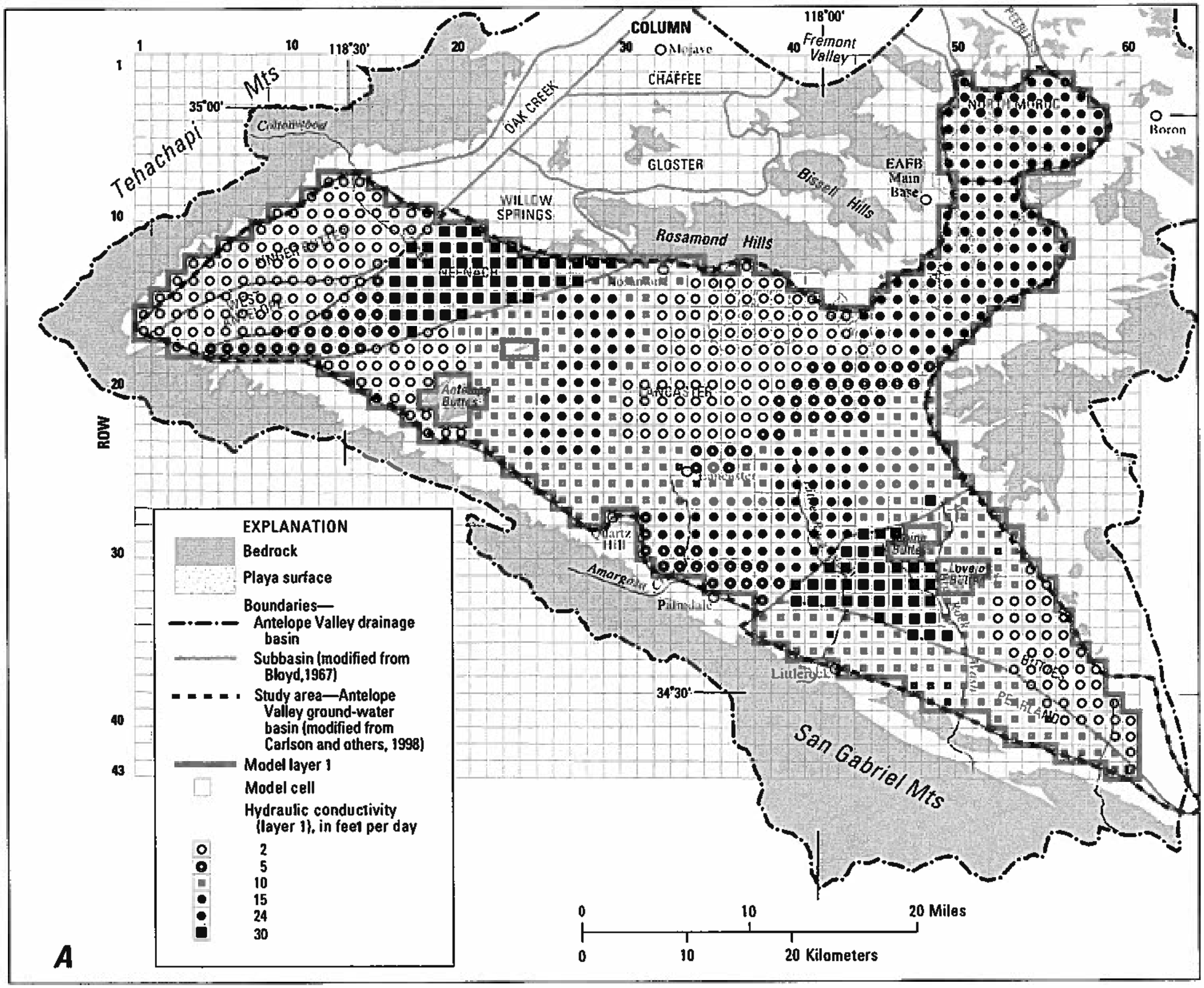

Figure 18. Areal distribution of *(A)* hydraulic conductivity for layer 1 and transmissivity for *(B)* layer 2 and *(C)* layer 3 in the ground-water flow model of the Antelope Valley ground-water basin, California.

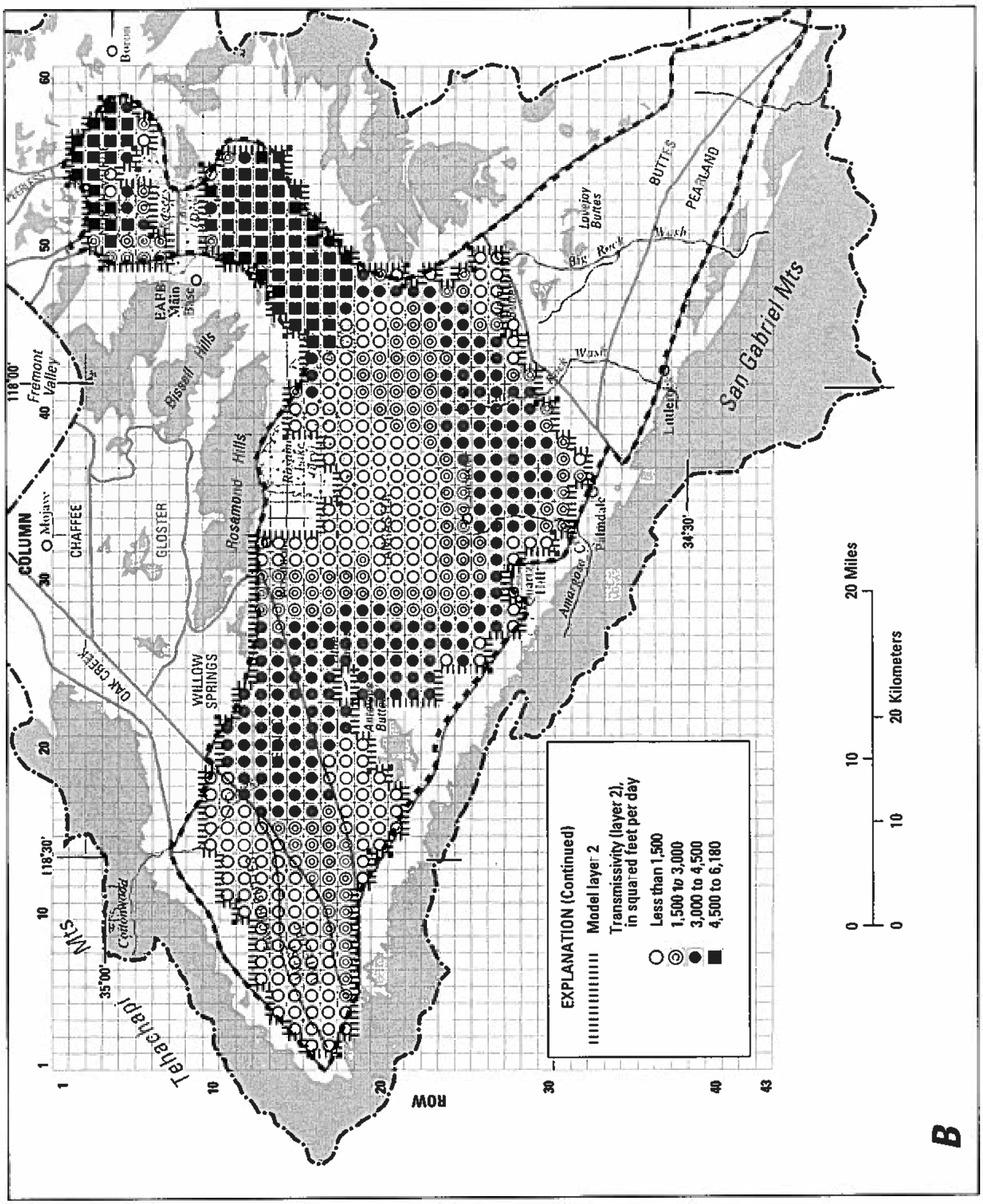

Figure 18.—Continued.

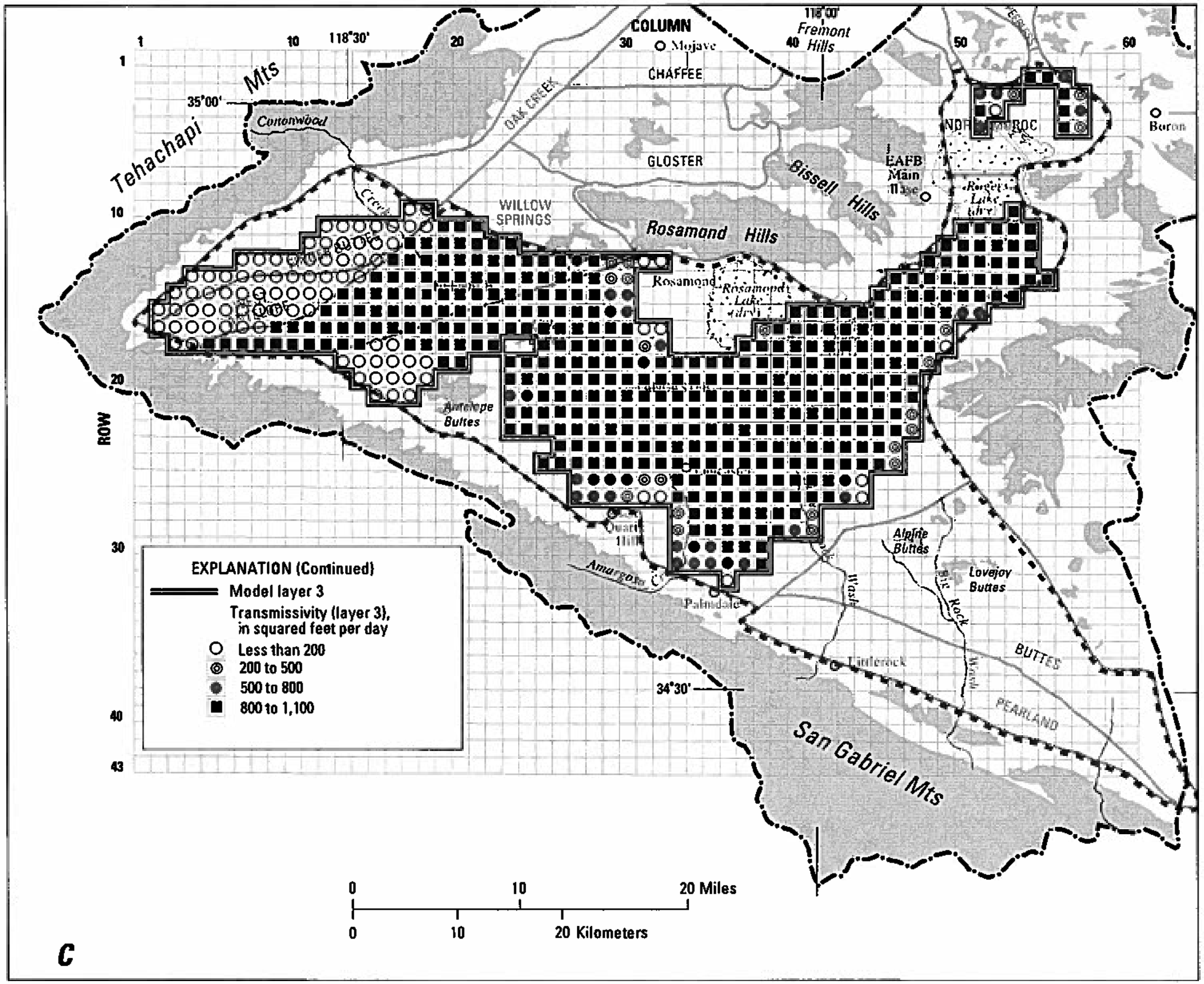

Figure 18.—Continued.

Transmissivity was specified for layers 2 and 3 in the model. Transmissivity was calculated outside the model using horizontal hydraulic conductivity and layer thickness. The horizontal hydraulic conductivity used to calculate the initial values of transmissivity for layer 2 was 10 ft/d. The thickness of layer 2 is 400 ft, except where the altitude of bedrock is higher than the 1,550 ft above sea level. During the calibration process, the horizontal hydraulic conductivity of layer 2 was adjusted in some areas to represent a distribution of sediments, which, in most cases, are coarse near the mountain fronts and fine near the valley center. For the area surrounding Rosamond Lake and south nearly to the city of Lancaster, the horizontal hydraulic conductivity used to calculate transmissivity for layer 2 was decreased to 2 ft/d. A transition zone having a horizontal hydraulic conductivity of 5 ft/d was specified between this area and the area to the south, which has a hydraulic conductivity of 10 ft/d. As required in layer 1, the horizontal hydraulic conductivity of layer 2 was decreased from 10 ft/d to 2 ft/d for the Finger Buttes and West Antelope subbasins and the western part of the Neenach subbasin. The horizontal hydraulic conductivity around the city of Palmdale was decreased from 10 ft/d to 5 ft/d to simulate the measured water-level declines in this area. Transmissivity for the area around Edwards Air Force Base was calculated using a horizontal hydraulic conductivity of 15 ft/d (Nishikawa and others, 2001). The calibrated transmissivities of layer 2 (fig. 18*B*) ranged from 11 to 6,000 ft^2/d.

The transmissivity of layer 3 was calculated using a hydraulic conductivity of 2 ft/d. The thickness of layer 3 is 550 ft, except where the altitude of bedrock is greater than 1,000 ft above sea level. The transmissivities of layer 3 (fig. 18*C*) ranged from 24 to 1,100 ft^2/d and were not adjusted during the calibration process.

The vertical leakance between layers was calculated outside of the model using equation 2. The vertical hydraulic conductivity of a layer that contains lacustrine deposits was assumed equal to 1.0×10^{-2} ft/d. The vertical hydraulic conductivity of a layer that does not contain lacustrine deposits was assumed equal to one-hundredth of the horizontal hydraulic conductivity of that layer. Vertical-leakance values were recalculated to reflect changes in horizontal hydraulic conductivity, transmissivity, and saturated thickness. The final calibrated values for vertical leakance ranged from 5.1×10^{-8} to 8.1×10^{-4} ft/d between layers 1 and 2 and from 7.1×10^{-6} to 1.04×10^{-4} ft/d between layers 2 and 3 (fig. 19). Calibration of vertical leakance in the model was difficult because the vertical hydraulic-head gradient has been measured at only a few sites.

Barriers to horizontal ground-water flow, such as faults, simulated in the model are shown in figure 11 and the final calibrated hydraulic characteristic values are presented in table 5. The hydraulic characteristic value of most of the faults simulated in this model initially were based on results from previous ground-water flow models [barriers 1–4 (Durbin, 1978) and barriers 5–7 (Nishikawa and others, 2001)]. The initial hydraulic-characteristic values of the barriers were modified during the calibration process to obtain acceptable water-level differences across the barriers. The northwest-southeast trending barrier (8), southeast of Lovejoy Buttes, was added to the model because the simulated water levels for well 6N/9W-11N1 (fig. 15) were consistently too high in the absence of a partial barrier to flow. Additional data are needed to verify the existence, location, and extent of this barrier. Barrier 9 (fig. 11) was added to the model to simulate the change in horizontal-flow characteristics where lacustrine deposits rise towards land surface and transect the upper and middle aquifers south of Rogers Lake (dry) (fig. 3). At this location, the lacustrine deposits may restrict the horizontal flow of ground water to areas of pumping to the south (Rewis, 1995, fig. 4). The delay and attenuated response, to pumpage, of water levels in well 8N/10W-8R3, located north of where the lacustrine deposits transect the upper and middle aquifers, compared to water levels in well 8N/11 W-34D2, located south of the lacustrine deposits, could not be simulated without simulating a partial barrier (barrier 9, fig. 11) to ground-water flow at this location.

Initial values of specific yield in layer 1 were adjusted for several parts of the study area during the calibration process. The specific-yield values specified for the Neenach subbasin (0.12), for some parts of the Lancaster subbasin (0.12), and for areas east and north of Rogers Lake (0.10) were decreased from initial values (0.15 to 0.20). The calibrated specific-yield value for the part of the Lancaster subbasin near Lancaster (0.12) is consistent with values estimated using coupled microgravity and water-level data (0.13) (Jim Howle, U.S. Geological Survey, written commun., 2002). The specific-yield value specified for the area around Rosamond Lake (0.10) was increased from the initial value (0.05). The final distribution of specific yield (layer 1) is shown in figure 20.

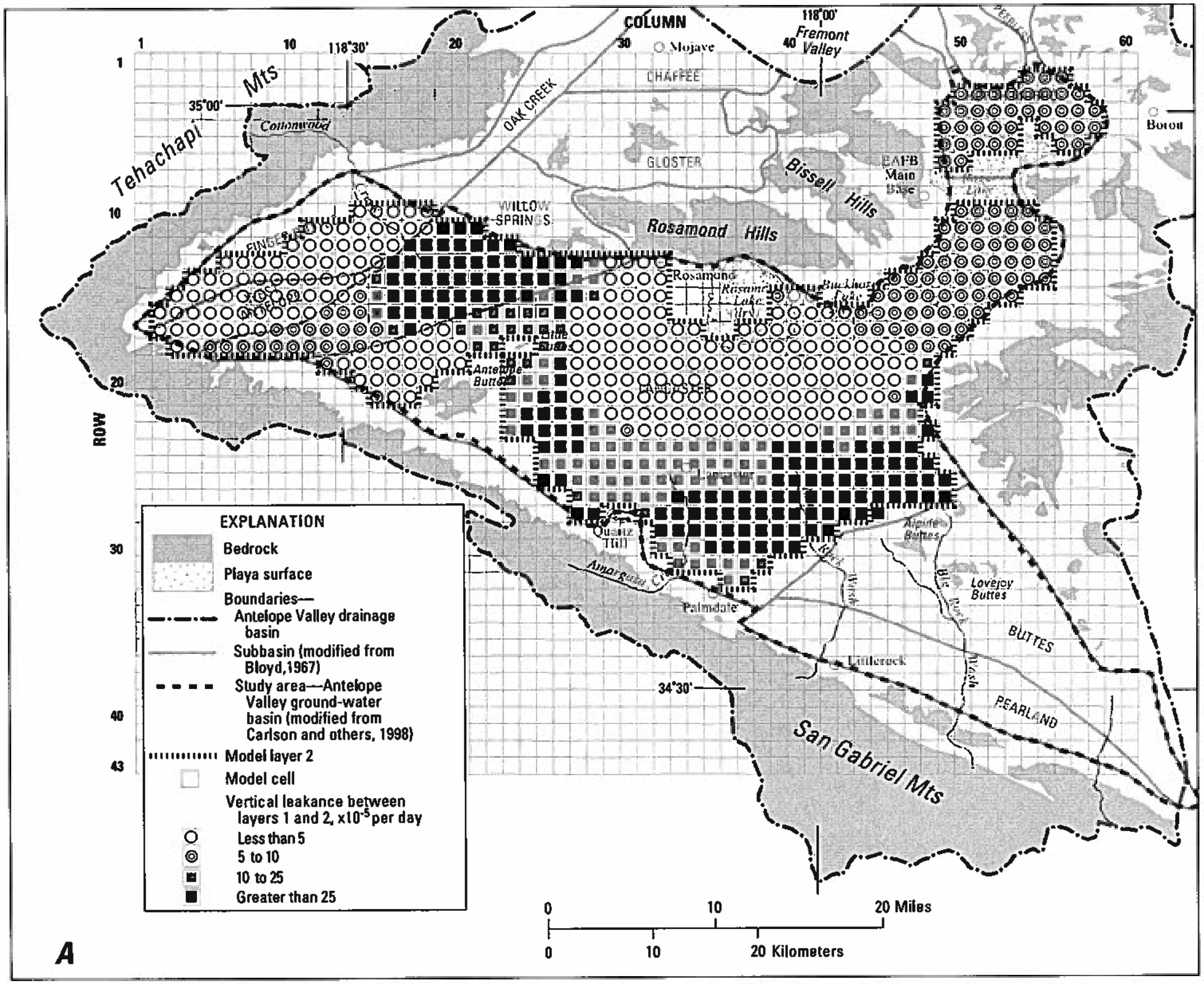

Figure 19. Areal distribution of vertical leakance between *(A)* layers 1 and 2 and *(B)* layers 2 and 3 in the ground-water flow model of the Antelope Valley ground-water basin, California.

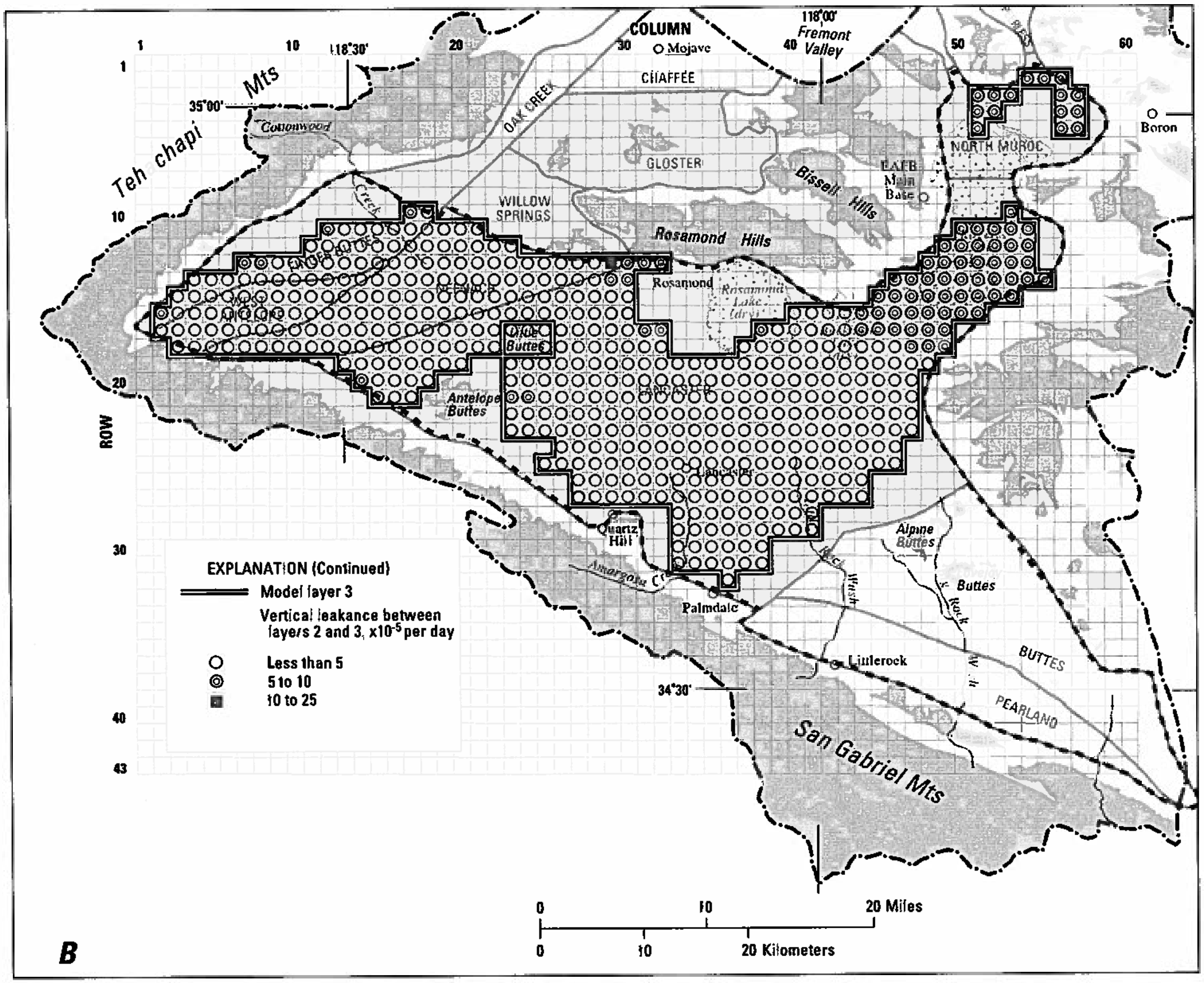

Figure 19.—Continued.

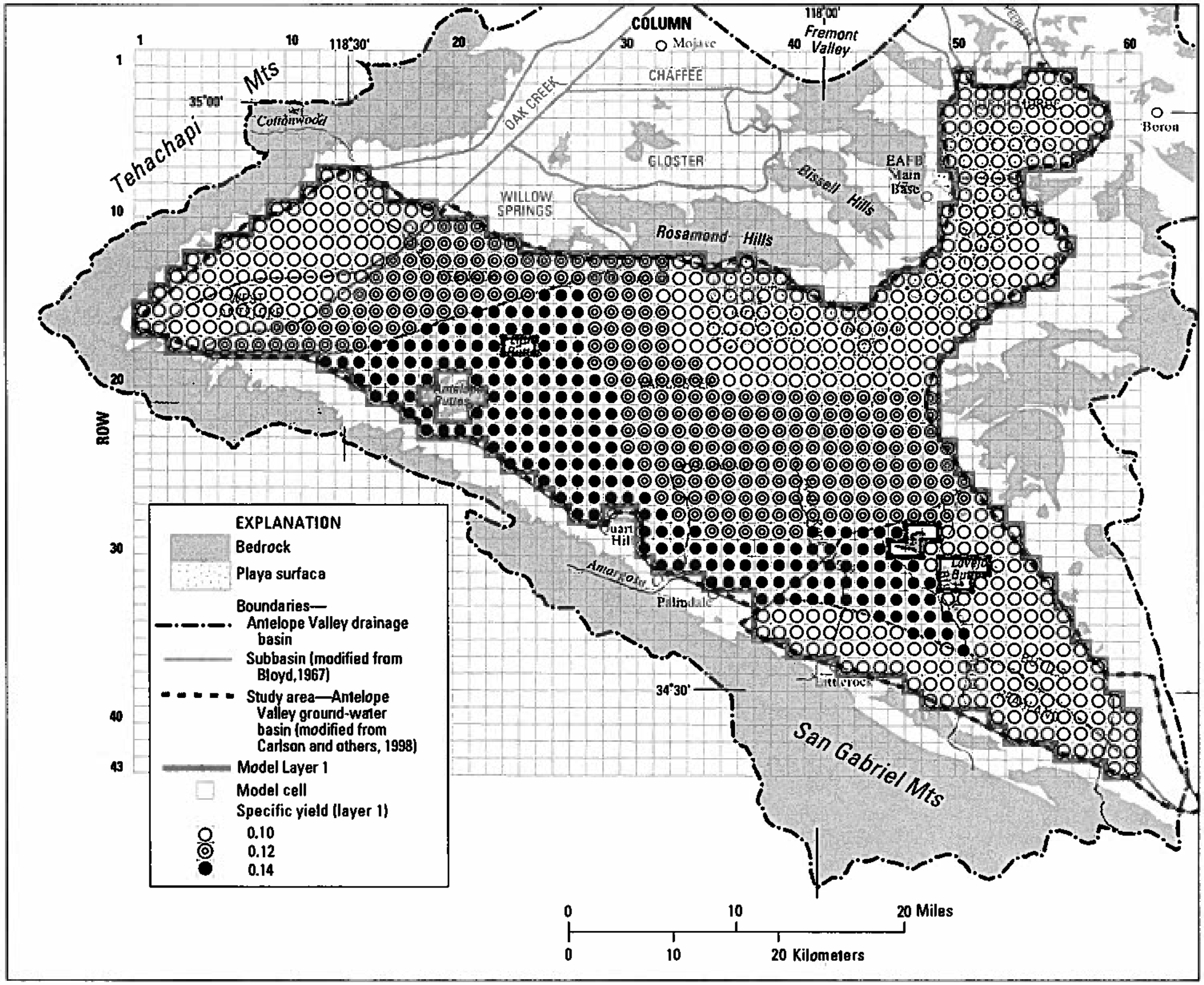

Figure 20. Areal distribution of specific yield in layer 1 of the ground-water flow model in the Antelope Valley ground-water basin, California.

The initial storage coefficients representing the compressibility of water and elastic skeletal storage were not changed during the calibration process. The storage coefficient representing the compressibility of water ranged from 0.3×10^{-4} to 5.1×10^{-4} in layer 1 (fig. 21*A*) and from 0.1×10^{-4} to 1.7×10^{-4} in layer 2 (fig. 21*B*), depending upon the thickness of saturated sediments in these layers. The elastic skeletal storage coefficient ranged from 1.0×10^{-4} to 2.07×10^{-3} in layer 1 (fig. 22*A*) and from 1.2×10^{-5} to 6.8×10^{-4} in layer 2 (fig. 22*B*). The final inelastic storage coefficient was calculated using an inelastic skeletal specific storage of 1.6×10^{-4} ft^{-1}, which is between the inelastic skeletal specific storage values for thick aquitards (3.5×10^{-4} ft^{-1}) and thin aquitards (4.0×10^{-5} ft^{-1}) reported by Sneed and Galloway (2000). The inelastic skeletal storage coefficient ranged from 2.9×10^{-3} to 3.11×10^{-2} in layer 1 (fig. 23*A*) and from 3.2×10^{-5} to 2.88×10^{-2} in layer 2 (fig. 23*B*). An inelastic skeletal storage coefficient was not specified for areas where subsidence has not been measured historically.

Calibrated preconsolidation head ranged from 0 to 160 ft below steady-state water levels in the area where subsidence was simulated (fig. 24). The preconsolidation head was adjusted until the timing of the onset of simulated subsidence matched measured subsidence. The variability in the calibrated preconsolidation head can be attributed to overconsolidation of the alluvium. Overconsolidlation of an alluvial basin can be caused by removal of overburden by erosion, prehistoric ground-water level declines, desiccation, and diagenesis (Holzer, 1981).

Irrigation-return flows were simulated as 30 percent of the annual quantity of water applied for agricultural irrigation. During the transient-state calibration process it was determined that irrigation-return flows recharged the underlying aquifer 10 years after the water was applied for irrigation. The calibrated delay between the application of irrigation water and the recharge of the irrigation-return flows was supported by the results of a simple unsaturated-zone model completed for this study using representative soil properties and depth to water measurements (Alan Flint, U.S. Geological Survey, written commun., 1999). Irrigation-return flows were applied directly to the model cells where agricultural pumping was simulated. In addition, irrigation-return flows were applied to the model cells where imported water was used for irrigation (fig. 12).

Model Results

Water Levels

Water-level hydrographs for 19 wells were used to compare simulated and measured water levels over time (fig. 25) (well locations shown on figure 15). The measured water levels for two wells (8N/10W-1Q3 and 8N/10W-4E1) were combined into one hydrograph to form a more complete period of record. The simulated water levels generally matched the trends of the measured water levels but did not always match the magnitude.

Twelve of the hydrographs compared simulated and measured water levels in the Lancaster subbasin. In general, the simulated water levels matched the measured water declines of more than 300 ft, which began in the 1920s, soon after pumpage exceeded estimates of natural recharge. In the southern part of the Lancaster subbasin (wells 6N/11W-19E6 and 7N/11W-31M1), the simulated water levels were more than 20 ft higher than the measured water levels after about 1970. In the western part of the Lancaster subbasin, east of Antelope Buttes (wells 7N/14W-13A1, 8N/13W-35M1, and 8N/14W-23G1), the simulated water levels generally were about 30 ft lower than the measured water levels. In the northeastern part of the Lancaster subbasin, the simulated water level in layer 3 at well 8N/10W-8R3 was about 20 ft lower than the measured water level after the late-1950s.